

Anomalous magnetization of a carbon nanotube as an excitonic insulator

Massimo Rontani*

CNR-NANO Research Center S3, Via Campi 213a, 41125 Modena, Italy

(Dated: May 9, 2018)

We show theoretically that an undoped carbon nanotube might be an excitonic insulator—the long-sought phase of matter proposed by Keldysh, Kohn and others fifty years ago. We predict that the condensation of triplet excitons, driven by intervalley exchange interaction, spontaneously occurs at equilibrium if the tube radius is sufficiently small. The signatures of exciton condensation are its sizeable contributions to both the energy gap and the magnetic moment per electron. The increase of the gap might have already been measured, albeit with a different explanation [V. V. Deshpande, B. Chandra, R. Caldwell, D. S. Novikov, J. Hone, and M. Bockrath, *Science* **323**, 106 (2009)]. The enhancement of the quasiparticle magnetic moment is a pair-breaking effect that counteracts the weak paramagnetism of the ground-state condensate of excitons. This property could rationalize the anomalous magnitude of magnetic moments recently observed in different devices close to charge neutrality.

PACS numbers: 73.63.Fg, 71.35.Lk, 71.35.Ji, 71.70.Gm

I. INTRODUCTION

After twenty years of intense investigation, carbon nanotubes (CNTs) still allow us to explore novel quantum physics in one dimension.^{1–6} The quality of suspended tubes⁷ achieved in transport measurements has disclosed subtle effects that previously had been obscured by sample disorder, such as spin-orbit interaction^{8–13} and Wigner localization.^{14,15} A growing body of experiments on single-wall CNTs shows that electron-electron interactions play a prominent role, being long-ranged and poorly screened close to charge neutrality. These observations include the emergence of an energy-gap of allegedly many-body origin in nominally metallic tubes,¹⁶ Wigner localization of excess charge carriers in semiconducting tubes,^{14,15} and the evidence of strong excitonic effects^{17–24}—even in metallic tubes.²⁵

The standard model of interacting electrons in CNTs is the Luttinger liquid,^{26,27} which was successful in explaining tunneling²⁸ and photoemission²⁹ spectra of metallic tubes. The reason is the perfect mapping of the linearly dispersive Tomonaga-Luttinger model onto the CNT effective-mass Hamiltonian,^{30,31} which at low energies exhibits the Dirac-Weyl form peculiar to massless fermions. However, this mapping becomes a poor approximation for undoped semiconducting tubes,^{32–34} since in the energy range close to band edges—where interactions are most effective—the noninteracting energy spectrum is massive and the Fermi level undefined. This is true even for nominally metallic tubes at half filling, due to the ubiquitous presence of small mass gaps induced by strain, twists, curvature,^{35,36} and spin-orbit coupling.^{37,38} The latter term affects also armchair tubes, whose metallicity is otherwise protected by symmetry.³⁵

Two alternative paradigms of strongly correlated insulators might fit carbon nanotubes. Intriguingly, both models were introduced by Mott long ago.^{39–41} The first concept is the Mott-Hubbard metal-insulator transition, which applies to solids that are metallic in the absence

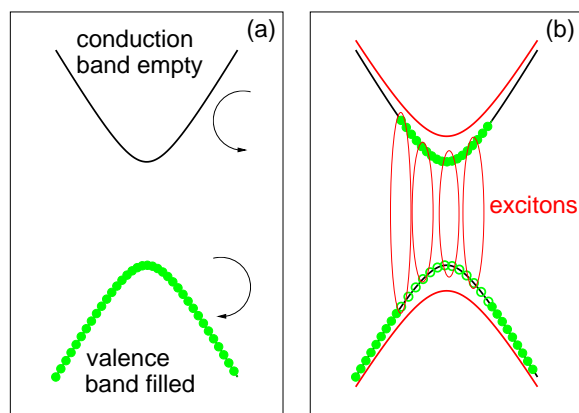


FIG. 1. (color online) Orbital magnetization of the exciton condensate. (a) Normal ground state of a metallic nanotube at finite magnetic field. The green [light gray] dots point to electrons filling the valence band. Conduction- and valence-band states exhibit opposite magnetic moments μ_0 , corresponding to either clockwise or anticlockwise rotations of electrons around the circumferential direction. The ground state is paramagnetic. (b) Excitonic insulator (EI) ground state. The magnetization of the EI phase is reduced with respect to that of the normal phase due to the spontaneous condensation of excitons. The thick red [gray] lines are the quasiparticle energy bands renormalized by the excitonic gap Δ .

of interactions.⁴² This scenario has been recently put forward^{30,43,44} to explain the many-body energy gap measured in half-filled CNTs.¹⁶ This quantity was obtained after subtracting the contributions to the transport gap due to finite-size effects and noninteracting mechanisms. We notice that the spin-orbit contribution to the energy gap was not considered by Ref. 16, despite the fact that it may be large¹² and cannot be fully compensated by the magnetic field in both spin channels (see Sec. XII).

The second paradigm is the excitonic insulator (EI)—the focus of this work—which applies to semiconductors exhibiting low dielectric screening and nested electron and hole Fermi surfaces.^{40,45–50} In the EI the strong attraction between electrons in the conduction band and holes in the valence band leads to the formation of excitons that undergo Bose-Einstein condensation, similarly to the way Cooper pairs condense in the Bardeen-Cooper-Schrieffer (BCS) ground-state. The outcome is a permanent insulating phase with energy gap enhanced by the remnant of the exciton binding energy Δ (see Fig. 1 and Ref. 51 for a recent review).

This scenario has been overlooked so far despite the strong evidence of major excitonic effects in CNTs.^{17–25} One important exception was the seminal 1997 paper by Ando,⁵² who realized that the electron-hole symmetry of CNT energy bands provides the perfect nesting for exciton condensation. However, he (and later Hartmann and coworkers⁵³) negated the stability of the EI phase on the basis of the energetics of spinless excitons.

Here, building on the investigations by Ando,^{52,54} we take a step forward and consider ‘dark’ triplet excitons, which have the lowest energy and are thought to play a prominent role in optical experiments.^{17,19–24,54–56} Contrary to previous work,^{53,54} we treat exchange interactions between electrons and holes in different valleys in a non-perturbative manner, as these interactions are poorly screened even for vanishing gap (the theory by Hartmann *et al.*⁵³ does not include the valley degree of freedom). Hence, including intervalley exchange forces from the beginning in a model Bethe-Salpeter equation that we solve exactly, we show that triplet excitons condense for sufficiently large values of intervalley exchange interaction and small radii. The resulting EI phase differs in many respects from that envisioned in the Sixties for semiconductors with parabolic bands,^{46–49} as a consequence of the relativistic dispersion of Dirac fermions and tube topology.

We predict that: (i) The stability of the EI is independent from the size of the noninteracting energy gap, which may be tuned e.g. by an axial magnetic field. (ii) The excitonic gap Δ adds quadratically to any noninteracting mass term, including the ubiquitous spin-orbit term. (iii) The quasiparticle magnetic moment, as observed by tunneling spectroscopy,⁵⁷ is enhanced with respect to its semiclassical value. This latter effect is due to the ionization of one of the excitons merging the condensate in order to release an unbound electron (hole) in the conduction (valence) band. Such ionization increases the total magnetization with respect to that of the ground state, which is a weak paramagnet (Fig. 1).

The above predictions may be experimentally validated as well as they may be used to extract the intervalley exchange strength, which is a fitting parameter in our theory. We stress that prediction (iii), which has no counterpart in the Mott-Hubbard scenario, might shed light on the anomalous magnitude of magnetic moments recently reported by different groups^{8,12,58,59} for devices

	Mott insulator	Excitonic insulator
Transport gap	opened	widened
Magnetic moment μ	unchanged	enhanced
Spin-orbit coupling	unchanged	enhanced
Subgap excitations	yes	yes

TABLE I. Mott-Hubbard versus excitonic insulators.

with very few carriers (cf. Table I and Sec. XII). Furthermore, prediction (ii) could explain the unusually large value of spin-orbit interaction measured by the Delft group,¹² which is presently not understood. Besides, the findings of Ref. 16 might be consistent with the EI scenario presented here, including the observation of subgap neutral excitations, as we further discuss in Sec. XII.

The reader not interested in the full derivation of our theory may skip the more technical sections and refer directly to the results illustrated in Secs. VII, X, XI, and XII. Sections II, III, and V review the results obtained by Ando in Refs. 52 and 54 as they are the starting point of our development, which is presented and discussed in the remaining part of the article.

The structure of this paper is as follows: We summarize the effective-mass theory of CNT single-particle states in Sec. II, which was the basis of the study of excitons by Ando. In Sec. III we recall his solution of the Bethe-Salpeter equation for spinless excitons within the random-phase approximation. We use Ando’s result to introduce a simpler two-band model for Dirac excitons in Sec. IV. We add spin and valley degrees of freedom in Sec. V and solve the corresponding Bethe-Salpeter equation for the triplet exciton in Sec. VI. We discuss the resulting excitonic instability in Sec. VII whereas in Sec. VIII we build the many-body theory of the EI and solve the gap equation in Sec. IX. Then in the following sections we present our main results: the anomalous enhancement of the magnetic moment per particle (Sec. X), the weak paramagnetism of the EI ground state (Sec. XI), and the relation to experiments (Sec. XII). After the conclusions (Sec. XIII), in Appendices A and B we work out respectively the Bethe-Salpeter and gap equations for semiconducting tubes in the presence of the magnetic field.

II. EFFECTIVE-MASS APPROXIMATION

In this section we recall the $\mathbf{k}\cdot\mathbf{p}$ theory of electronic π -states in single-wall carbon nanotubes (CNTs) according to Ando.^{52,54,60}

Carbon nanotubes may be thought of as wrapped sheets of graphene, hence nanotube electronic states are built from those of graphene after imposing suitable boundary conditions. Here we focus on single-particle levels lying close to K (isospin $\tau = 1$) or K’ ($\tau = -1$) points in graphene’s reciprocal space, where Dirac cones’

apexes touch. These two apexes are the Fermi surface of undoped graphene. The envelope functions $\mathbf{F}^\tau(\mathbf{r})$ of CNT single-particle states are two-component spinors, each component being the wave function amplitude on one of the two sublattices. These envelopes obey the $\mathbf{k} \cdot \mathbf{p}$ equations of graphene,

$$\gamma(\sigma_x \hat{k}_x + \tau \sigma_y \hat{k}_y) \mathbf{F}^\tau(\mathbf{r}) = \varepsilon \mathbf{F}^\tau(\mathbf{r}), \quad (1)$$

plus the additional boundary condition along the tube circumference:

$$\mathbf{F}^\tau(\mathbf{r} + \mathbf{L}) = \mathbf{F}^\tau(\mathbf{r}) \exp \left[2\pi i \left(\varphi - \tau \frac{\nu}{3} \right) \right]. \quad (2)$$

Here \mathbf{L} is the chiral vector in the circumference direction of the CNT, $\nu = 0, \pm 1$ is the chirality index that depends on the microscopic structure of the CNT ($\nu = 0$ for metals and $\nu = \pm 1$ for semiconductors), $\varphi = \phi/\phi_0$ is the ratio of the magnetic flux ϕ through the tube cross section to the magnetic flux quantum $\phi_0 = ch/e$, γ is graphene's band parameter, σ_x and σ_y are the Pauli matrices, ε is the single-particle energy, $\hat{k}_x = -i\partial/\partial x$ is the wave vector operator along the circumference direction x and $\hat{k}_y = -i\partial/\partial y$ acts on the tube axis coordinate y .

The energy bands are specified by the index $\alpha = (n, \ell)$ plus the wave vector k in the axis direction, where n is an integer and $\ell = c, v$ denotes either the conduction ($\ell = c$) or the valence band ($\ell = v$). The wave functions in the K valley are

$$\mathbf{F}_{\alpha k}^{\text{K}}(\mathbf{r}) = \boldsymbol{\xi}_{\alpha k}^{\text{K}}(x) \frac{1}{\sqrt{A}} \exp(iky), \quad (3)$$

where A is the CNT length and the wave function $\boldsymbol{\xi}_{\alpha k}^{\text{K}}(x)$ for the motion along the circumference direction is

$$\boldsymbol{\xi}_{\alpha k}^{\text{K}}(x) = \frac{1}{\sqrt{L}} \exp[ik_\nu(n)x] \mathbf{F}_{\alpha k}^\nu, \quad (4)$$

with $L = |\mathbf{L}|$ being the tube circumference. In Eq. (4) the transverse wave vector $k_\nu(n)$ depends on the magnetic flux,

$$k_\nu(n) = \frac{2\pi}{L} \left(n + \varphi - \frac{\nu}{3} \right), \quad (5)$$

and the spinor $\mathbf{F}_{\alpha k}^\nu$ is a unit vector with a \mathbf{k} -dependent phase between the two sublattice components,

$$\mathbf{F}_{\alpha k}^\nu = \frac{1}{\sqrt{2}} \begin{pmatrix} b_\nu(n, k) \\ s_\alpha \end{pmatrix}, \quad (6)$$

where

$$b_\nu(n, k) = \frac{k_\nu(n) - ik}{\sqrt{k_\nu^2(n) + k^2}}, \quad (7)$$

and $s_\alpha = \pm 1$ for conduction and valence bands, respectively. The corresponding energy is

$$\varepsilon_\alpha^{\text{K}}(k) = s_\alpha \gamma \sqrt{k_\nu^2(n) + k^2}, \quad (8)$$

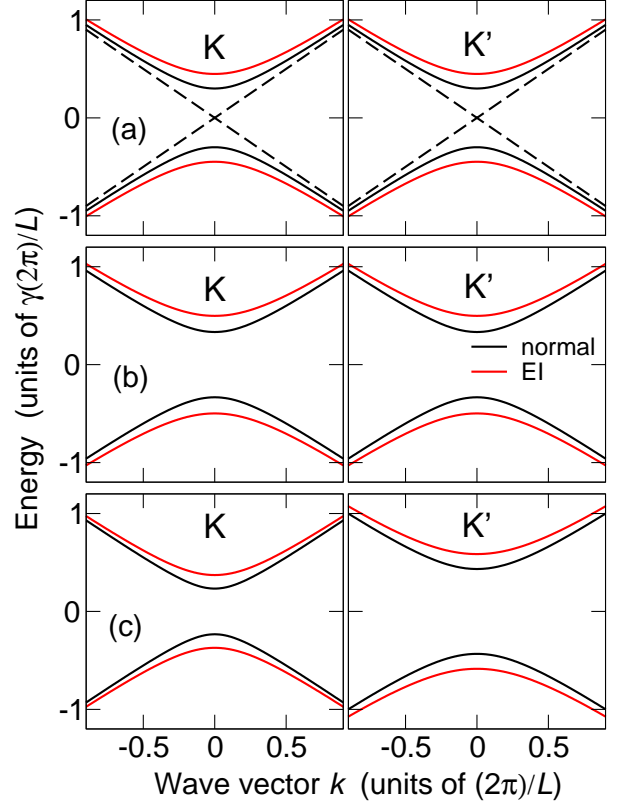


FIG. 2. (color online) Dispersion of electronic energy levels of single-wall carbon nanotubes close to the charge neutrality point. The dependence of the energy on wave vector k in both valleys K (left column) and K' (right column) is shown. Black (red [gray]) lines represent noninteracting (EI quasiparticle) energy bands $\varepsilon^\tau(k)$ [$E^\tau(k)$]. (a) Metallic tube in the presence of the magnetic flux $\varphi = 0.3$. Here $\varphi = \phi/\phi_0$ is the ratio of the magnetic flux ϕ through the tube cross section to the magnetic flux quantum $\phi_0 = ch/e$. The dashed line is the dispersion with $\varphi = 0$. (b) Semiconducting tube with $\nu = 1$ and $\varphi = 0$. (c) Semiconducting tube with $\nu = 1$ and $\varphi = 0.1$. As the field along the tube axis is increased the gap in valley K' increases while the gap in valley K decreases. Quasiparticle energies are obtained from their weak-coupling expressions for the sake of comparison among all panels, with $a(2\pi/L) = 1$ and $w_2 = 100\gamma(2\pi/L)$.

which is reckoned from the charge neutrality point (Fig. 2).

The wave function in the K' valley is

$$\mathbf{F}_{\alpha k}^{\text{K}'}(\mathbf{r}) = \boldsymbol{\xi}_{\alpha k}^{\text{K}'}(x) \frac{1}{\sqrt{A}} \exp(iky), \quad (9)$$

with

$$\boldsymbol{\xi}_{\alpha k}^{\text{K}'}(x) = \frac{1}{\sqrt{L}} \exp[ik_{-\nu}(n)x] \mathbf{F}_{\alpha k}^{-\nu*}, \quad (10)$$

whereas its energy is

$$\varepsilon_\alpha^{\text{K}'}(k) = s_\alpha \gamma \sqrt{k_{-\nu}^2(n) + k^2}. \quad (11)$$

III. BETHE-SALPETER EQUATION FOR SPINLESS EXCITONS

In this section we recall Ando's results for spinless excitons in a single valley⁵² to validate a simpler two-band model that is at the basis of our further development.

The exciton wave function $|u\rangle$ of zero center-of-mass momentum in the—say—K valley is

$$|u\rangle = \sum_n \sum_k \psi_n(k) \hat{c}_{n,c,k}^{K+} \hat{c}_{n,v,k}^K |g\rangle, \quad (12)$$

where $|g\rangle$ is the ground state of the intrinsic CNT with all v bands filled and c bands empty, $\psi_n(k)$ is the n th component of the exciton wave function in the reciprocal space, and the operator $\hat{c}_{n,c,k}^{K+}$ creates an electron in valley K having conduction-band index n and momentum k . There are no off-diagonal contributions with different band indices in (12) since these are forbidden by the symmetry of Coulomb interaction [cf. (13)].

The Bethe-Salpeter equation for the exciton wave function $\psi_n(k)$ of eigenvalue ε_u is:

$$\begin{aligned} \varepsilon_u \psi_n(k) &= [\varepsilon_{n,c}^K(k) - \varepsilon_{n,v}^K(k) + \Delta\varepsilon_n^K(k)] \psi_n(k) \\ &- \sum_{m,q} V_{(n,c,k;m,c,k+q)(m,v,k+q;n,v,k)} \psi_m(k+q). \end{aligned} \quad (13)$$

Here $\varepsilon_{n,c}^K(k) - \varepsilon_{n,v}^K(k) = 2\gamma [k_\nu^2(n) + k^2]^{1/2}$ is the energy cost for creating a noninteracting electron of momentum k in the n th conduction band and a hole the n th valence band, $\Delta\varepsilon_n^K(k)$ is the sum of electron and hole quasiparticle self-energies due to interaction, and $V_{(n,c,k;m,c,k+q)(m,v,k+q;n,v,k)}$ is the screened Coulomb matrix element that scatters different electron-hole pairs, binding the electron and the hole. The above quantities were evaluated by Ando within the random phase approximation and the eigenvalue problem (13) was solved numerically, as detailed in Ref. 52.

Ando considered generic CNTs exhibiting a gap, i.e., both semiconductors ($\nu = \pm 1$) and metals ($\nu = 0$) in the presence of the magnetic field ($\varphi \neq 0$). He found that the terms related to Coulomb interaction appearing on the right hand side of the Bethe-Salpeter equation (13)—the self-energy $\Delta\varepsilon^K$ and the matrix element V —are large taken separately, because of the reduced dimensionality of the CNT and its poor screening. However, these two terms cancel out almost exactly, hence the binding energy lowers the exciton level below the quasiparticle band edge of continuum states while the self-energy lifts the band edge above its noninteracting value. The net effect is that the energy of the lowest exciton level, ε_u , is slightly blueshifted with respect to the bare energy gap, $2\gamma |k_\nu(0)|$, and redshifted with respect to the interacting energy gap, E_g . Since the exciton energy is always positive, $\varepsilon_u > 0$, Ando concluded that an excitonic instability never occurs [Fig. 3(a)]. A similar result was inferred by Hartmann and coworkers on the basis of a semianalytical model.⁵³

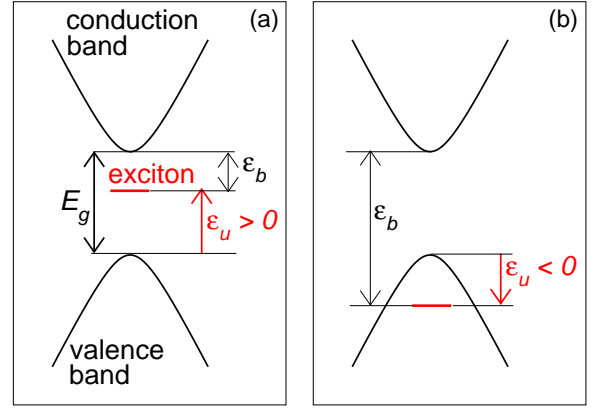


FIG. 3. (color online) Excitonic instability. (a) In the ordinary case the excitation energy ε_u of the exciton is positive and smaller than the quasiparticle gap E_g . The exciton binding energy ε_b is smaller than E_g . (b) An excitonic instability occurs for $\varepsilon_u < 0$ ($\varepsilon_b > E_g$), which drives the transition to the excitonic insulator phase.

To derive a simpler exciton model, we use the key result by Ando that the lowest exciton energy ε_u is homogeneous and almost linear with the gap E_g , as shown in Fig. 5 of Ref. 52 for metallic CNTs as a function of the magnetic field that opens the gap. The rationale is that the smaller the band gap the stronger the screening, which makes the exciton binding energy approximately proportional to the gap. Besides, ε_u weakly depends on the strength of Coulomb interaction, $(e^2/\varepsilon_r L)/(2\pi\gamma/L)$, as seen in Fig. 4 of Ref. 52 showing that ε_u is almost constant for reasonable values of $(e^2/\varepsilon_r L)/(2\pi\gamma/L) > 0.1$. Here, the quantity $(e^2/\varepsilon_r L)/(2\pi\gamma/L)$ is dimensionless, with $(e^2/\varepsilon_r L)/(2\pi\gamma/L) = 0.3545/\varepsilon_r$, ε_r being the unknown static dielectric constant describing contributions from states far from the charge neutrality point, and $2\pi\gamma/L$ being the energy unit.

On the basis of the results plotted in Figs. 4 and 5 of Ref. 52 that we have recalled above, we approximate ε_u as

$$\varepsilon_u \approx \beta E_g, \quad (14)$$

where E_g is the band gap renormalized by Coulomb interaction—possibly in the presence of the magnetic field—and β is a fraction of the unity, $\beta \approx 0.8$.

IV. TWO-BAND MODEL FOR SPINLESS EXCITONS

Next we introduce a simpler two-band model that reproduces the numerical result (14) for the lowest exciton state. This model will be the starting point of our theory.

We consider only the lowest conduction and highest valence band, labeled by $n = 0$ for moderate values of φ ,

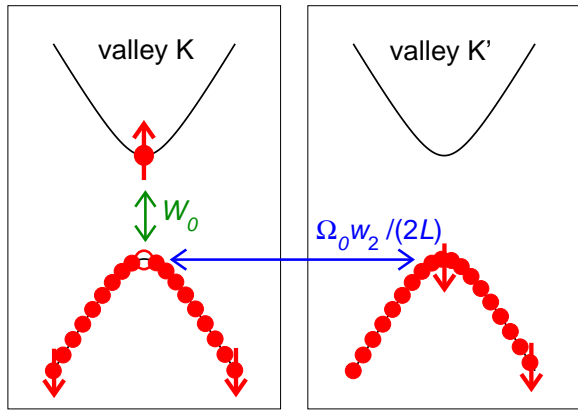


FIG. 4. (color online) Two-band model for the lowest triplet exciton. W_0 is the intravalley interaction energy and $\Omega_0 w_2 / 2L$ is the intervalley exchange interaction. The arrows represent electron spins. Here the exciton spin projection is $S_z = 1$.

so the exciton wave function is

$$|u\rangle = \sum_k \psi(k) \hat{c}_{c,k}^{K+} \hat{c}_{v,k}^K |g\rangle, \quad (15)$$

with the shorthands $\psi(k) \equiv \psi_{n=0}(k)$ and $\hat{c}_{c,k}^{K+} \equiv \hat{c}_{0,c,k}^{K+}$. The Bethe-Salpeter equation takes the form

$$\left[2\gamma \sqrt{k_\nu(0)^2 + k^2} + \Delta\varepsilon(k) \right] \psi(k) - \sum_q V_{k;k+q} \psi(k+q) = \varepsilon_u \psi(k). \quad (16)$$

Furthermore, we assume that: (i) the effect of the self-energy $\Delta\varepsilon(k)$ may be included into the band structure by renormalizing the band parameter γ (ii) the screened Coulomb matrix element $V_{k;k+q}$ does not depend on momenta, $V_{k;k+q} \equiv W_0/A$ with $W_0 > 0$ (cf. Fig. 4). The former assumption implies that the value of γ should be estimated through a quasiparticle calculation, like the GW technique. The latter approximation provides a contact attractive interaction that captures the essential physical features of excitons in CNTs.^{17,56}

We proceed Fourier transforming (16) in real space,

$$2\gamma \sqrt{k_\nu(0)^2 - \frac{d^2}{dy^2}} \psi(y) - W_0 \delta(y) \psi(y) = \varepsilon_u \psi(y), \quad (17)$$

with $\psi(y)$ being the exciton wave function for the relative motion of the electron-hole pair. The square root operator appearing in (17) is a symbolic expression for the power series

$$\sqrt{k_\nu(0)^2 - \frac{d^2}{dy^2}} = |k_\nu(0)| + |k_\nu(0)| \sum_{n=1}^{\infty} \binom{1/2}{n} \frac{(-1)^n}{|k_\nu(0)|^{2n}} \frac{d^{(2n)}}{dy^{(2n)}}. \quad (18)$$

It is tempting to keep only the second derivative in the expansion on the right hand side of (18), thus recovering the familiar Wannier equation for a massive exciton in an usual semiconductor.⁴⁶ However, later we will be interested in exploring the excitonic instability (Fig. 3), which is the critical regime that one reaches at the frontier of the domain of convergence of the power series (18). Therefore we fully take into account the relativistic dispersion of the exciton—a peculiar feature of CNTs—and solve exactly (17). Our approach allows for a solution also in the supercritical regime $\varepsilon_u < 0$, as we will discuss in Sec. VII, contrary to the method illustrated in Ref. 53. Both relativistic and nonrelativistic treatments provide the same results for small ratios of W_0 to γ .

As in the nonrelativistic case, the solution of (17) is a bound state whose wave function $\psi(y)$ takes the form

$$\psi(y) = \sqrt{\kappa} \exp(-\kappa |y|), \quad (19)$$

and whose energy ε_u is smaller than the gap $E_g = 2\gamma |k_\nu(0)|$,

$$\varepsilon_u = 2\gamma \sqrt{k_\nu(0)^2 - \kappa^2}. \quad (20)$$

Here the exciton inverse decay length $\kappa > 0$ has to be determined through the proper boundary condition at the origin. This condition is obtained by integrating both sides of (17) over an infinitesimal interval containing the origin, providing

$$-4\gamma |k_\nu(0)| \sum_{n=1}^{\infty} \binom{1/2}{n} \frac{(-1)^n}{|k_\nu(0)|^{2n}} \kappa^{2n-1} = W_0, \quad (21)$$

which may be resummed as

$$\gamma \sqrt{k_\nu(0)^2 - \kappa^2} = \gamma |k_\nu(0)| - \frac{\kappa W_0}{4}. \quad (22)$$

Resolving (22) for κ one obtains

$$\kappa = \frac{8\gamma |k_\nu(0)| W_0}{16\gamma^2 + W_0^2}, \quad (23)$$

therefore the exciton energy is:

$$\varepsilon_u = 2\gamma |k_\nu(0)| \frac{16\gamma^2 - W_0^2}{16\gamma^2 + W_0^2}. \quad (24)$$

As expected, the attractive contact interaction W_0 lowers ε_u below the band gap E_g .

The value of W_0 is determined imposing the constraint (14), which provides

$$W_0 = 4 \sqrt{\frac{1-\beta}{1+\beta}} \gamma \approx 1.33 \gamma. \quad (25)$$

The latter estimate corresponds to $\beta = 0.8$. The parameter β weakly depends on the strength of Coulomb interaction for realistic values of ϵ_r . We see that γ is the only energy scale that appears in the equation of motion (17) for a Dirac exciton in a single valley.

V. EXCHANGE INTERACTION

Whereas in Secs. III and IV we have focused on excitons whose electron and hole constituents occupy the K valley (KK exciton), we may consider as well excitons in the K' valley (K'K' exciton) and excitons made of the electron in the K valley and hole in the K' valley (KK' exciton) or vice versa (K'K exciton). Including the spin degree of freedom, there is a total amount of sixteen different excitons made of an electron in the valley τ with spin σ and a hole in the valley τ' with spin σ' , that we label as $|(\tau, \sigma)(\tau', \sigma')\rangle$, with $\tau, \tau' = \text{K or K}'$ and $\sigma, \sigma' = \uparrow$ or \downarrow (here we comply with the notation by Ando⁵⁴ that the spin of the hole is denoted by that of the missing electron in the valence band).

These excitons, which are all degenerate in the absence of the magnetic field, may be further classified in terms of the total spin as singlet and triplet excitons. There are four singlet excitons,

$$^1|\tau\tau'\rangle = \frac{1}{\sqrt{2}} [|(\tau, \uparrow)(\tau', \uparrow)\rangle + |(\tau, \downarrow)(\tau', \downarrow)\rangle], \quad (26)$$

and four triplet excitons that are separately threefold degenerate due to the different spin projections $S_z = +1, 0, -1$,

$$\begin{aligned} ^3|\tau\tau', +1\rangle &= |(\tau, \uparrow)(\tau', \downarrow)\rangle, \\ ^3|\tau\tau', 0\rangle &= \frac{1}{\sqrt{2}} [|(\tau, \uparrow)(\tau', \uparrow)\rangle - |(\tau, \downarrow)(\tau', \downarrow)\rangle], \\ ^3|\tau\tau', -1\rangle &= |(\tau, \downarrow)(\tau', \uparrow)\rangle. \end{aligned} \quad (27)$$

In the following we take into account the orbital coupling with the magnetic field through the transverse wave vector $k_\nu(0)$ but neglect the small Zeeman coupling lifting spin degeneracies S_z .

Ando has showed that the sixteen-fold degeneracy of the exciton manifold is lifted by the small short-range part of Coulomb interaction, which is not included in the $\mathbf{k} \cdot \mathbf{p}$ theory^{54,61} and is responsible for spin and valley exchange. Intervalley exchange interaction splits singlet states into the bonding and antibonding of $^1|\text{KK}\rangle$ and $^1|\text{K}'\text{K}'\rangle$ and two degenerate $^1|\text{KK}'\rangle$ and $^1|\text{K}'\text{K}\rangle$. Triplet excitons split in the same way although each triplet is three-fold degenerate. The overall ordering and energy splitting is determined by two exchange parameters, w_1 and w_2 .

The generic lowest exciton state turns out to be the triplet 'bonding' exciton,

$$\frac{1}{\sqrt{2}} [^3|\text{KK}, S_z\rangle + ^3|\text{K}'\text{K}', S_z\rangle] \quad \text{with } S_z = -1, 0, 1, \quad (28)$$

which is optically inactive (Fig. 4). The energy of this bonding exciton is lower than that of the single-valley KK or K'K' excitons due to intervalley exchange. This prediction agrees with available state-of-art fully ab-initio calculations.^{17,56} Since we are concerned with ground-state properties only, we will limit our study to the triplet exciton (28) focusing on its specific equation of motion.

The short-range part of Coulomb interaction has both an intravalley and an intervalley contribution, respectively $\hat{V}^{(1)}$ and $\hat{V}^{(2)}$. The matrix element of $\hat{V}^{(1)}$ has the form

$$\Omega_0 w_1 \int d\mathbf{r} [\mathbf{F}_{\alpha_1 k_1}^\tau(\mathbf{r})^\dagger \sigma_z \mathbf{F}_{\alpha_2 k_2}^\tau(\mathbf{r})] [\mathbf{F}_{\alpha_3 k_3}^{\tau'}(\mathbf{r})^\dagger \sigma_z \mathbf{F}_{\alpha_4 k_4}^{\tau'}(\mathbf{r})], \quad (29)$$

where $\Omega_0 = (\sqrt{3}/2)a^2$ is the area of graphene unit cell, $a = 2.46 \text{ \AA}$ is the lattice constant, and $w_1 > 0$ characterizes intravalley interaction strength. The matrix element of $\hat{V}^{(2)}$ is

$$\begin{aligned} \Omega_0 w_2 \int d\mathbf{r} [&\mathbf{F}_{\alpha_1 k_1}^{\tau A}(\mathbf{r})^* \mathbf{F}_{\alpha_2 k_2}^{\tau' A}(\mathbf{r}) \mathbf{F}_{\alpha_3 k_3}^{\tau' A}(\mathbf{r})^* \mathbf{F}_{\alpha_4 k_4}^{\tau A}(\mathbf{r}) \\ &+ \mathbf{F}_{\alpha_1 k_1}^{\tau B}(\mathbf{r})^* \mathbf{F}_{\alpha_2 k_2}^{\tau' B}(\mathbf{r}) \mathbf{F}_{\alpha_3 k_3}^{\tau' B}(\mathbf{r})^* \mathbf{F}_{\alpha_4 k_4}^{\tau B}(\mathbf{r})], \end{aligned} \quad (30)$$

where $\tau \neq \tau'$, the apex A (B) labels the first (second) spinorial sublattice component, and $w_2 > 0$ characterizes intervalley interaction strength (cf. Fig. 4). We expect that the effect of screening on matrix elements (29) and (30) is smaller than that on the conventional long-range Coulomb terms discussed in Sec. III, hence we neglect it.⁵⁴

The exchange terms $\hat{V}^{(1)}$ and $\hat{V}^{(2)}$ pertinent to the two-band model introduced in Sec. IV take the form

$$\begin{aligned} \hat{V}^{(1)} &= \frac{\Omega_0 w_1}{2AL} \sum_{\tau\tau'} \sum_{\alpha\beta\alpha'\beta'} \sum_{kk'q} \sum_{\sigma\sigma'} \\ &\times V_{(\tau, \alpha, k+q; \tau\beta, k)(\tau', \beta', k'; \tau', \alpha', k'+q)}^{(1)} \\ &\times \hat{c}_{\alpha, k+q, \sigma}^{\tau+} \hat{c}_{\beta', k', \sigma'}^{\tau'+} \hat{c}_{\alpha', k'+q, \sigma'}^{\tau'} \hat{c}_{\beta, k, \sigma}^{\tau}, \end{aligned} \quad (31)$$

and

$$\begin{aligned} \hat{V}^{(2)} &= \frac{\Omega_0 w_2}{2AL} \sum_{\tau \neq \tau'} \sum_{\alpha\beta\alpha'\beta'} \sum_{kk'q} \sum_{\sigma\sigma'} \\ &\times V_{(\tau', \alpha, k+q; \tau\beta, k)(\tau, \beta', k'; \tau', \alpha', k'+q)}^{(2)} \\ &\times \hat{c}_{\alpha, k+q, \sigma}^{\tau'+} \hat{c}_{\beta', k', \sigma'}^{\tau'+} \hat{c}_{\alpha', k'+q, \sigma'}^{\tau'} \hat{c}_{\beta, k, \sigma}^{\tau}, \end{aligned} \quad (32)$$

where $\hat{c}_{\beta, k, \sigma}^{\tau}$ destroys an electron in the valley τ with momentum k and spin σ occupying either the conduction ($\beta = c$) or valence ($\beta = v$) band $n = 0$. Explicitly, the matrix elements are

$$\begin{aligned} &V_{(\tau, \alpha, k+q; \tau\beta, k)(\tau', \beta', k'; \tau', \alpha', k'+q)}^{(1)} \\ &= \frac{1}{4} [b_\nu^*(0, k+q) b_\nu(0, k) - s_\alpha s_\beta] \\ &\times [b_{-\nu}(0, k') b_{-\nu}^*(0, k'+q) - s_{\beta'} s_{\alpha'}] \end{aligned} \quad (33)$$

and

$$\begin{aligned} &V_{(\tau', \alpha, k+q; \tau\beta, k)(\tau, \beta', k'; \tau', \alpha', k'+q)}^{(2)} \\ &= \frac{1}{4} [b_{-\nu}(0, k+q) b_\nu(0, k) b_\nu^*(0, k') b_{-\nu}^*(0, k'+q) \\ &+ s_\alpha s_\beta s_{\beta'} s_{\alpha'}]. \end{aligned} \quad (34)$$

These matrix elements are further simplified taking $k, k', q \approx 0$, in the spirit of the $\mathbf{k} \cdot \mathbf{p}$ method. Then (33) is 1

if $(\alpha \neq \beta) \wedge (\alpha' \neq \beta')$ and zero otherwise, (34) is $1/2$ if $s_\alpha s_\beta s_{\beta'} s_{\alpha'} = 1$ and zero otherwise. The term (32), responsible for intervalley exchange, is the only short-range contribution relevant to the dynamics of the triplet exciton (28), as we discuss below.

VI. BETHE-SALPETER EQUATION FOR THE LOWEST TRIPLET EXCITON

In this section we extend the two-band model of Sec. IV adding spin and valley degrees of freedom to treat the lowest triplet exciton (28). The generic wave function of this exciton is

$$|u\rangle = \sum_{\tau,k} \psi_\tau(k) \hat{c}_{c,k,\uparrow}^{\tau+} \hat{c}_{v,k,\downarrow}^{\tau-} |g\rangle. \quad (35)$$

Here we consider both metallic and semiconducting nanotubes and choose the spin projection $S_z = 1$ for the sake of clarity, as illustrated in Fig. 4.

The short-range terms that enter the equation of motion must scatter the electron-hole pairs $\hat{c}_{c,k,\uparrow}^{\tau+} \hat{c}_{v,k,\downarrow}^{\tau-} |g\rangle$ that span the triplet exciton subspace. The intravalley operator $\hat{V}^{(1)}$ unaffected this subspace—at least at the lowest order—except for a small negative constant term lowering the exciton energy that may be neglected.⁵⁴ On the other hand, the intervalley operator $\hat{V}^{(2)}$ transfers electron-hole pairs from one valley to the other one, whereas the diagonal term is the same for both ground and exciton states (Fig. 4). The resulting equations of motion, Fourier transformed in real space, are:

$$\begin{aligned} \varepsilon_u \psi_K(y) &= 2\gamma \sqrt{k_\nu(0)^2 - \frac{d^2}{dy^2}} \psi_K(y) - W_0 \delta(y) \psi_K(y) \\ &\quad - \frac{\Omega_0 w_2}{2L} \delta(y) \psi_{K'}(y) \\ \varepsilon_u \psi_{K'}(y) &= 2\gamma \sqrt{k_{-\nu}(0)^2 - \frac{d^2}{dy^2}} \psi_{K'}(y) - W_0 \delta(y) \psi_{K'}(y) \\ &\quad - \frac{\Omega_0 w_2}{2L} \delta(y) \psi_K(y). \end{aligned} \quad (36)$$

Equations (36) provide the bound state of a two-component massive exciton with a relativistic dispersion. In the relative-motion frame of (36) two types of attractive scattering potentials occur at the origin—the coordinate at which the electron and the hole share the same position along the CNT axis. One contact term is due to intravalley Coulomb interaction with strength W_0 and the other one to intervalley exchange with strength $\Omega_0 w_2/2L$, as shown in Fig. 4.

The solution of (36) is straightforward in the case the gaps in the two valleys are identical, $|k_\nu(0)| = |k_{-\nu}(0)|$ (black line in Fig. 5). This occurs for either a metallic CNT ($\nu = 0$) at any field [Fig. 2(a)] or a semiconducting tube ($\nu = \pm 1$) at zero field [Fig. 2(b)] (see Appendix A for the generic solution). Then the components of the exciton in the two valleys are identical as

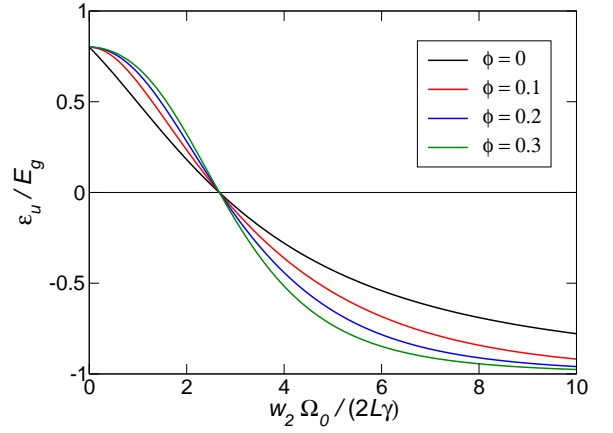


FIG. 5. (color online) Energy ε_u of the lowest triplet exciton vs exchange interaction strength $(\Omega_0 w_2/2L)/\gamma$ for different magnetic field fluxes φ . The black line represents the energy of either a metallic tube ($\nu = 0$) at any field or a semiconducting tube ($\nu = \pm 1$) at zero field. Colored [gray] lines correspond to $\nu = \pm 1$ and finite field. Here $\varphi = \phi/\phi_0$ is the ratio of the magnetic flux ϕ through the tube cross section to the magnetic flux quantum $\phi_0 = ch/e$. The energy ε_u is in units of the quasiparticle gap E_g , with $E_g = 2\gamma |k_{\nu=0}(0)|$ for a metal and $E_g = \min(2\gamma |k_{\nu=1}(0)|, 2\gamma |k_{\nu=-1}(0)|)$ for a semiconductor. At the critical value of interaction $\Omega_0 w_2/2L + W_0 = 4\gamma$ the exciton energy becomes negative (here $W_0 = 1.33\gamma$).

well, $\psi_K(y) = \psi_{K'}(y)$, their explicit form being given by (19) after replacing W_0 with $W_0 + \Omega_0 w_2/2L$. The exciton energy is

$$\varepsilon_u = 2\gamma |k_\nu(0)| \frac{16\gamma^2 - [W_0 + (\Omega_0 w_2/2L)]^2}{16\gamma^2 + [W_0 + (\Omega_0 w_2/2L)]^2}, \quad (37)$$

which is the same as the spinless result (24) except for the key difference that the exchange interaction strength $\Omega_0 w_2/2L$ now adds to W_0 .

For semiconductors at finite field the exciton energy is obtained numerically, as shown in Fig. 5 (colored [gray] lines). As the mismatch between the band edges of valleys K and K' increases with the field (φ increases) the exciton binding energy decreases (ε_u increases).

VII. EXCITONIC INSTABILITY

Whereas the intravalley interaction strength W_0 weakly depends on tube parameters, the exchange interaction strength $\Omega_0 w_2/2L$ that enters the exciton energy (37) depends on the inverse of tube circumference L as well as on the microscopic details of the interaction potential and exciton wave function through the parameter w_2 (Ref. 54). As shown in Fig. 5, at the critical value

$$W_0 + \frac{\Omega_0 w_2}{2L} = 4\gamma \quad (38)$$

the excitation energy ε_u goes to zero, thus the ‘normal’ ground state $|g\rangle$ becomes unstable against the sponta-

neous formation of triplet excitons.

This scenario, proposed in the Sixties by Mott,⁴⁰ Keldysh,⁴⁵ and Kohn⁴⁷ among others, is illustrated in Fig. 3(b). In the supercritical regime $\varepsilon_u < 0$ the ground state rearranges itself into the long-sought ‘excitonic insulator’ (EI) phase. The EI phase, which is pictorially depicted in Fig. 1(b), is a permanent condensate of excitons at thermodynamic equilibrium exhibiting insulating behavior. The quasiparticle gap (red [gray] lines in Figs. 2 and 1) is widened with respect to the normal ground state due to the emergence of a many-body contribution Δ reminiscent of the exciton binding energy [see Eq. (51) below].

Using the estimate by Ando⁵⁴ of $w_2 \approx 4$ eV, Eq. (25), and taking $\gamma = 5.39$ eV·Å we obtain as a critical value of the tube circumference $L = 0.73$ Å, which is at least one order of magnitude smaller than realistic values. However, quoting Ando,⁵⁴ ‘It is worth being pointed out that the parametrization into w_1 and w_2 is much more general although their actual values can be different from those estimated above [...] we should leave w_1 and w_2 rather as adjustable parameters to be determined experimentally’. In much the same spirit, we propose that the observable properties of the excitonic insulator should be used to extract the value of w_2 .

Beyond the critical value of exchange interaction, $W_0 + \Omega_0 w_2 / 2L > 4\gamma$, the exciton energy ε_u becomes negative according to (37), which is at odds with the square-root dependence of the kinetic energy in (17) only allowing for positive values of ε_u [cf. Eq. (20)]. This issue is related to the problem of supercritical fields in quantum electrodynamics,⁶² which has received a great deal of attention in the context of graphene^{63–66} and carbon nanotubes.^{53,67} In the present context, we note that the sum of the infinite series defining the kinetic energy operator on the rhs of (18) is a double valued function. Taking the negative square root and repeating the calculation of Sec. IV we obtain that the formulae (23), (24), (37) for both the exciton inverse decay length κ and energy ε_u are analytically continued in the supercritical regime ($\varepsilon_u < 0$).

The exciton energy ε_u in the whole range of exchange interaction is plotted in Fig. 5. The binding energy $\varepsilon_b = |2\gamma|k_\nu(0)| - \varepsilon_u|$ in the supercritical regime becomes larger than the gap $2\gamma|k_\nu(0)|$, reaching its maximum allowed value of twice the gap, $4\gamma|k_\nu(0)|$, at infinite exchange interaction ($\varepsilon_u/E_g = -1$). Therefore, contrary to the case of relativistic electron states in superheavy atoms, the exciton bound level never merges the antiparticle continuum lying at the bottom of the forbidden energy gap, located at $-2\gamma|k_\nu(0)|$ (not to be confused with the top of the valence band). This prediction is in striking contrast with the conclusions of Hartmann and coworkers.⁵³

VIII. EXCITONIC INSULATOR

In this section we build up the Hartree-Fock theory of the EI phase of carbon nanotubes, which significantly departs from the treatment of usual semiconductors^{46–50} due to the relativistic character and chirality of electrons. We include in our two-band Hamiltonian \hat{H} only those terms responsible for the excitonic instability,

$$\hat{H} = \hat{H}_0 + \hat{V}_{\text{intra}} + \hat{V}_{\text{inter}}, \quad (39)$$

where \hat{H}_0 is the noninteracting term,

$$\hat{H}_0 = \sum_{\tau, \alpha, k, \sigma} \varepsilon_\alpha^\tau(k) \hat{c}_{\alpha, k, \sigma}^{\tau+} \hat{c}_{\alpha, k, \sigma}^\tau, \quad (40)$$

\hat{V}_{intra} is the intravalley interaction term introduced in Sec. IV,

$$\hat{V}_{\text{intra}} = \frac{W_0}{A} \sum_{\tau} \sum_{kk'q} \sum_{\sigma\sigma'} \hat{c}_{c, k+q, \sigma}^{\tau+} \hat{c}_{v, k'-q, \sigma'}^{\tau+} \hat{c}_{v, k', \sigma'}^\tau \hat{c}_{c, k, \sigma}^\tau, \quad (41)$$

and \hat{V}_{inter} is the intervalley exchange term discussed in Sec. V,

$$\hat{V}_{\text{inter}} = \frac{\Omega_0 w_2}{2AL} \sum_{\tau \neq \tau'} \sum_{kq} \sum_{\sigma\sigma'} \hat{c}_{c, k+q, \sigma}^{\tau'+} \hat{c}_{v, k, \sigma'}^{\tau'+} \hat{c}_{v, k+q, \sigma'}^\tau \hat{c}_{c, k, \sigma}^\tau. \quad (42)$$

Furthermore, we introduce the intraband one-particle Green function,

$$G_{\sigma\sigma'}^\alpha(\tau k, t) = -i\hbar^{-1} \left\langle T \left\{ \hat{c}_{\alpha, k, \sigma}^\tau(t) \hat{c}_{\alpha, k, \sigma'}^{\tau+}(0) \right\} \right\rangle, \quad (43)$$

as well as the ‘anomalous’ interband Green function,

$$F_{\sigma\sigma'}^{\alpha\beta}(\tau k, t) = -i\hbar^{-1} \left\langle T \left\{ \hat{c}_{\alpha, k, \sigma}^\tau(t) \hat{c}_{\beta, k, \sigma'}^{\tau+}(0) \right\} \right\rangle. \quad (44)$$

The latter is zero for the noninteracting ground state but takes a finite value in the EI phase, pointing to electron-hole interband correlations (here $\alpha\beta = cv$ or vc). In (43) and (44) T is the time-ordering operator and $\langle \dots \rangle$ the quantum average over the ground state.⁶⁸

Whereas the intraband Green function is diagonal in the spin space as the EI ground state has no net spin magnetization,

$$G_{\sigma\sigma'}^\alpha(\tau k, t) = \delta_{\sigma\sigma'} G^\alpha(\tau k, t), \quad (45)$$

the interband Green function is spin-polarized along the (arbitrary) direction \mathbf{n} ,

$$F_{\sigma\sigma'}^{\alpha\beta}(\tau k, t) = (\mathbf{n} \cdot \boldsymbol{\sigma})_{\sigma\sigma'} F^{\alpha\beta}(\tau k, t), \quad (46)$$

with $\boldsymbol{\sigma}$ being the vector formed by the three Pauli matrices and \mathbf{n} a constant unit vector. This may be understood as $F_{\sigma\sigma'}^{cv}(\tau k, 0+)$ is proportional to the wave function in reciprocal space of the condensate of triplet excitons whose spins are polarized along \mathbf{n} . This condensate

has no macroscopic magnetization but exhibits a periodic modulation of the spin density within each unit cell of the honeycomb lattice (antiferromagnetic spin density wave).^{46,48} Whereas the long range order of the spin density wave is destroyed by quantum and thermal fluctuations in an indefinitely long tube, here we assume the size of the sample is comparable to the spin-spin correlation length.

We obtain the Fourier-transformed quantities $G^\alpha(\tau k, \omega)$ and $F^{\alpha\beta}(\tau k, \omega)$ from their Heisenberg equations of motion after applying the Hartree-Fock decoupling scheme.⁴⁷ The system of equations involving $G^c(\tau k, \omega)$ is

$$\begin{aligned} [\hbar\omega - \varepsilon_c^\tau(k)] G^c(\tau k, \omega) - \Delta(\tau k) F^{vc}(\tau k, \omega) &= 1 \\ [\hbar\omega - \varepsilon_v^\tau(k)] F^{vc}(\tau k, \omega) - \Delta^*(\tau k) G^c(\tau k, \omega) &= 0, \end{aligned} \quad (47)$$

where we have introduced the gap function $\Delta(\tau k)$ defined through the equation

$$\begin{aligned} \Delta^*(\tau k) &= \frac{i\hbar}{A} \sum_q \left[W_0 F^{vc}(\tau k + q, t = 0+) \right. \\ &\quad \left. + \frac{\Omega_0 w_2}{2L} F^{vc}(-\tau k + q, t = 0+) \right], \end{aligned} \quad (48)$$

with $-\tau$ labeling the valley different from τ . The equations involving $G^v(\tau k, \omega)$ do not provide additional information. Solving system (47) for G^c and F^{vc} in terms of Δ , we obtain

$$G^c(\tau k, \omega) = \frac{\hbar\omega - \varepsilon_v^\tau(k)}{[\hbar\omega - \varepsilon_c^\tau(k)][\hbar\omega - \varepsilon_v^\tau(k)] - |\Delta(\tau k)|^2}, \quad (49)$$

$$F^{vc}(\tau k, \omega) = \frac{\Delta^*(\tau k)}{[\hbar\omega - \varepsilon_c^\tau(k)][\hbar\omega - \varepsilon_v^\tau(k)] - |\Delta(\tau k)|^2}. \quad (50)$$

The poles of Green functions (49) and (50) are the (spin-degenerate) quasiparticle energies $E^\tau(k)$ (Ref. 68). These bands are plotted in Figs. 2 and 1 (red [gray] lines), their explicit form being given by

$$\begin{aligned} E^K(k) &= \pm \sqrt{\gamma^2 k_\nu^2(0) + \gamma^2 k^2 + |\Delta(Kk)|^2}, \\ E^{K'}(k) &= \pm \sqrt{\gamma^2 k_{-\nu}^2(0) + \gamma^2 k^2 + |\Delta(K'k)|^2}, \end{aligned} \quad (51)$$

where the sign plus and minus refers to electrons and holes, respectively. The result (51) shows that the valley-dependent gap function $|\Delta(\tau k)|$ adds quadratically to the noninteracting half-gap, $\gamma |k_{\pm\nu}(0)|$. Substituting (50) into (48) and integrating over the frequency we obtain the gap equation,

$$\begin{aligned} \Delta(\tau k) &= \frac{1}{A} \sum_q \left[W_0 \frac{\Delta(\tau k + q)}{2 |E^\tau(k + q)|} \right. \\ &\quad \left. + \frac{\Omega_0 w_2}{2L} \frac{\Delta(-\tau k + q)}{2 |E^{-\tau}(k + q)|} \right], \end{aligned} \quad (52)$$

which implicitly provides $|\Delta(\tau k)|$. This equation has the same structure as the gap equation of BCS theory of

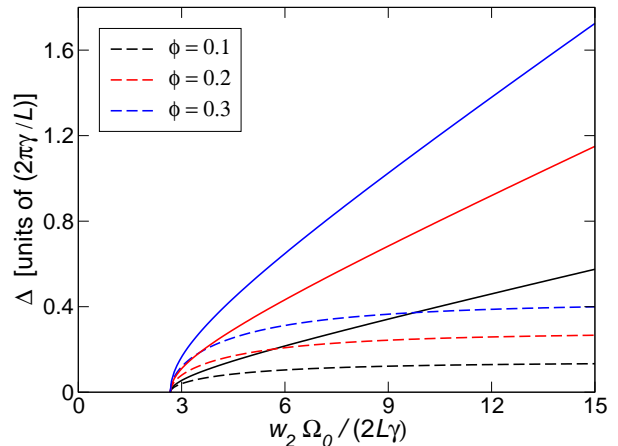


FIG. 6. (color online) Excitonic gap Δ of a nominally metallic tube ($\nu = 0$) vs interaction strength $(\Omega_0 w_2 / 2L) / \gamma$ at zero temperature for different values of the magnetic flux φ . The dashed lines are the values obtained by a weak-coupling expansion. Here $\varphi = \phi / \phi_0$ is the ratio of the magnetic flux ϕ through the tube cross section to the magnetic flux quantum $\phi_0 = ch/e$ and $W_0 = 1.33\gamma$.

superconductivity.^{69,70} Excluding the trivial noninteracting solution $\Delta(\tau k) = 0$, a finite value of $\Delta(\tau k)$ points to the stability of the EI phase with respect to the noninteracting ground state. The phase of $\Delta(\tau k)$ is arbitrary and the energy is independent of it.

IX. SOLUTION OF THE GAP EQUATION

To solve the gap equation (52) we assume that the excitonic gap function $\Delta(\tau k)$ is independent from k , $\Delta(\tau k) \equiv \Delta(\tau)$, and rewrite (52) as

$$\begin{aligned} &2\sqrt{\gamma^2 k_\nu^2(0) + \gamma^2 k^2 + |\Delta(K)|^2} \varphi^K(k) \\ &= \frac{1}{A} \sum_q \left[W_0 \varphi^K(k + q) + \frac{\Omega_0 w_2}{2L} \varphi^{K'}(k + q) \right], \\ &2\sqrt{\gamma^2 k_{-\nu}^2(0) + \gamma^2 k^2 + |\Delta(K')|^2} \varphi^{K'}(k) \\ &= \frac{1}{A} \sum_q \left[W_0 \varphi^{K'}(k + q) + \frac{\Omega_0 w_2}{2L} \varphi^K(k + q) \right], \end{aligned} \quad (53)$$

with the position $\varphi^\tau(k) = \Delta(\tau) / 2 |E^\tau(k)|$. We see that for a vanishing value of the excitonic gap—at the border of the EI phase, $\Delta(\tau) = 0+$, the gap equation coincides with the Bethe-Salpeter equation (36) in momentum space for the triplet exciton of zero energy. This confirms that at the critical interaction strength (38) the nanotube undergoes a transition to the EI phase (Fig. 6).

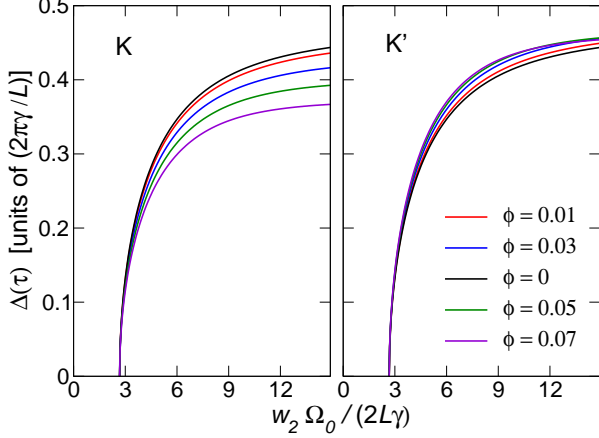


FIG. 7. (color online) Excitonic gap $\Delta(\tau)$ of a semiconducting tube ($\nu = 1$) vs interaction strength $(\Omega_0 w_2/2L)/\gamma$ for different values of the magnetic flux φ . The data refer to zero temperature and weak coupling. Left panel: valley K. Right panel: valley K'. Here $\varphi = \phi/\phi_0$ is the ratio of the magnetic flux ϕ through the tube cross section to the magnetic flux quantum $\phi_0 = ch/e$ and $W_0 = 1.33\gamma$.

A. Weak coupling

There are two ways of solving the gap equation (53). The first method is valid only at weak coupling, i.e., the excitonic gap is much smaller than the noninteracting gap, $|\Delta(\tau)| \ll \gamma |k_\nu(0)|$, hence we may expand the square root entering (53) in terms of $|\Delta(\tau)|$ (Ref. 46). In the case of either metallic tubes or semiconducting tubes at zero field the gaps in the two valleys are equal, $\Delta(K) = \Delta(K') \equiv \Delta$, hence at the lowest order (53) reduces to

$$\begin{aligned} 2\gamma\sqrt{k_\nu^2(0) + k^2}\varphi(k) - \frac{1}{A}\sum_q \left[W_0 + \frac{\Omega_0 w_2}{2L} \right] \varphi(k+q) \\ = -\frac{|\Delta|^2}{\gamma |k_\nu(0)|} \varphi(k), \end{aligned} \quad (54)$$

with $\varphi^\tau \equiv \varphi$. This is identical to the Bethe-Salpeter equation (36) for a triplet exciton of energy $-|\Delta|^2/\gamma |k_\nu(0)|$. Equating this latter energy to (37) and solving for $|\Delta|$, we obtain

$$|\Delta| = \sqrt{2}\gamma |k_\nu(0)| \sqrt{\frac{[W_0 + (\Omega_0 w_2/2L)]^2 - 16\gamma^2}{[W_0 + (\Omega_0 w_2/2L)]^2 + 16\gamma^2}} \quad (55)$$

for $W_0 + \Omega_0 w_2/2L \geq 4\gamma$ and $|\Delta| = 0$ otherwise (dashed lines in Fig. 6). The generic weak-coupling case of a valley-dependent excitonic gap $\Delta(\tau)$ for semiconducting tubes at finite field is worked out in Appendix B and illustrated in Fig. 7.

The dependence of $|\Delta|$ on both the exchange interaction strength $\Omega_0 w_2/2L$ and noninteracting gap width $2\gamma |k_\nu(0)|$ tuned by the field is displayed in Fig. 6 (dashed

lines). The excitonic gap $|\Delta|$ is zero below the critical threshold of intervalley exchange interaction and increases up to the maximum value of $\sqrt{2}\gamma |k_\nu(0)|$ at strong interaction strength. Beyond the critical threshold, the EI phase is stable for any size of the noninteracting bandgap. The latter is tuned by the magnetic field, the excitonic gap vanishing with the noninteracting gap.

This scaling of excitonic and noninteracting gaps—a consequence of the relativistic dispersion of Dirac electrons—is in striking contrast with the behavior of the EI gap predicted for ordinary semiconductors.⁴⁶ In this latter case the onset of EI phase occurs when, decreasing the size of noninteracting gap e.g. by applying pressure to the solid, the band gap equals the exciton binding energy, which only depends on the exciton mass and dielectric constant.

B. Strong coupling

In the strong-coupling limit of arbitrary exchange interaction strength, $\Omega_0 w_2/2L$, we directly perform the sum over q in (52), limiting ourselves to the case of valley-independent Δ . This sum exhibits an unphysical ultraviolet divergence that originates from the assumed independence of Δ from k . Therefore, we introduce the cutoff k_c in the summation (52). The fact that Δ vanishes at the critical interaction strength (38) provides a constraint that fixes the value of k_c . The result is

$$k_c = \sinh \frac{\pi}{2} |k_\nu(0)| \approx 2.301 |k_\nu(0)|, \quad (56)$$

scaling with the noninteracting gap. Note that (56) compares with the cutoff value $2\pi/L$ taken in the numerical calculations of Ref. 52. After performing the integration of (53), the generic form of Δ is

$$\Delta = \gamma |k_\nu(0)| \left[\frac{\sinh\left(\frac{\pi}{2}\right)^2}{\sinh\left(\frac{2\pi\gamma}{W_0 + \Omega_0 w_2/(2L)}\right)^2} - 1 \right]^{1/2} \quad (57)$$

for $W_0 + \Omega_0 w_2/(2L) > 4\gamma$ and $\Delta = 0$ otherwise.

The strong-coupling value of Δ given by (57) is compared with the weak-coupling prediction in Fig. 6 (solid versus dashed lines, respectively). Whereas the two families of curves overlap close to the critical interaction strength, the strong-coupling value approximately doubles its weak-coupling counterpart around $w_2\Omega_0/(2L\gamma) \sim 6$, increasing unboundedly with interaction strength.

The effect of temperature T on the excitonic gap Δ may be evaluated straightforwardly, paralleling the procedure of BCS theory.⁷⁰ The T -dependent gap equation is

$$\begin{aligned} \frac{2\pi\gamma}{W_0 + \Omega_0 w_2/(2L)} = \int_0^{\sinh(\pi/2)} \frac{dt}{(1 + \tilde{\Delta}^2 + t^2)^{1/2}} \\ \times \tanh \left[\frac{\tilde{\beta}}{2} (1 + \tilde{\Delta}^2 + t^2)^{1/2} \right], \end{aligned} \quad (58)$$

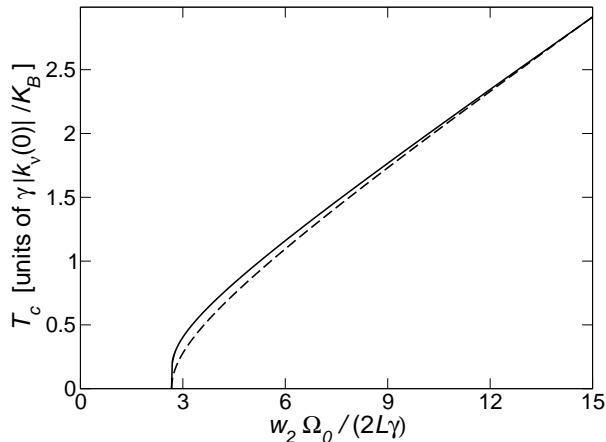


FIG. 8. Critical temperature T_c vs interaction strength $(\Omega_0 w_2 / 2L) / \gamma$ (solid line). The temperature scales linearly with $\gamma |k_\nu(0)|$, i.e., half the noninteracting gap. The noninteracting tube is either metallic ($\nu = 0$) in the presence of the magnetic field or semiconducting ($\nu = \pm 1$) in the absence of the field. Here K_B is Boltzmann constant and $W_0 = 1.33\gamma$. For comparison, the excitonic gap at $T = 0$, $\Delta(T = 0) / (\gamma |k_\nu(0)| K_B)$, rescaled by the factor 0.5067, is shown as a dashed line.

where we have defined the reduced quantities $\tilde{\Delta} = \Delta(T) / (\gamma |k_\nu(0)|)$ and $\tilde{\beta} = \beta \gamma |k_\nu(0)|$, with $\beta = 1 / (K_B T)$ and K_B is the Boltzmann constant. The critical temperature T_c is obtained putting $\tilde{\Delta} = 0$ into (58) and then solving numerically the corresponding equation, which provides the relation between T_c and interaction strength.

The outcome is shown in Fig. 8. As it is evident from the comparison between T_c (solid line) and the excitonic gap at zero temperature $\Delta(T = 0)$, rescaled by the factor 0.5067 (dashed line), both curves share approximately the same dependence on $\Omega_0 w_2 / 2L$, at least for strong interaction. Therefore, the equation

$$K_B T_c \approx 0.507 \Delta(T = 0) \quad (59)$$

provides a useful estimate of the effect of temperature. Since typical small-gap semiconducting tubes exhibit transport gaps—possibly of excitonic origin—of the order of tens of meV whereas measurements are performed around $T \approx 100$ mK,^{12,16} one may neglect the effect of temperature at the first instance.

This is confirmed by the temperature dependence of $\Delta(T)$, which is illustrated in Fig. 9. Similarly to the gap in BCS theory, close to $T = 0$ the excitonic gap $\Delta(T)$ exhibits a large plateau whereas in the neighborhood of T_c it drops with a square-root dependence. Therefore, $\Delta(T)$ is substantially unaffected by T in a broad range of cryogenic temperatures relevant for experiments. In the remaining part of the paper we will neglect temperature effects.

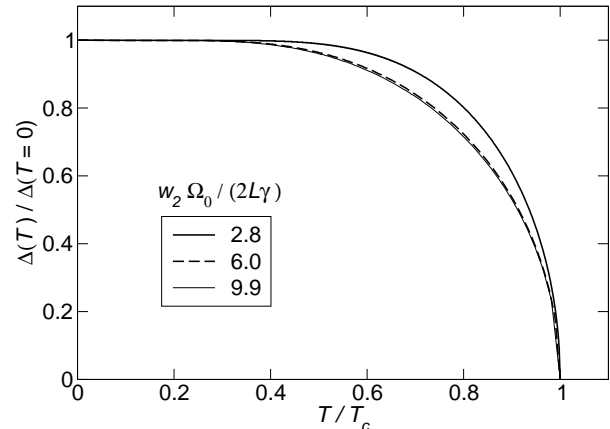


FIG. 9. Normalized excitonic gap $\Delta(T) / \Delta(T = 0)$ vs normalized temperature T / T_c for different values of interaction strength $(\Omega_0 w_2 / 2L) / \gamma$. The noninteracting tube is either metallic ($\nu = 0$) in the presence of the magnetic field or semiconducting ($\nu = \pm 1$) in the absence of the field.

X. EXCITONIC ENHANCEMENT OF THE QUASIPARTICLE MAGNETIC MOMENT

From the knowledge of the quasiparticle energy $E^\tau(k)$ it is straightforward to compute the magnetic moment per quasiparticle, μ , defined as the negative slope of the quasiparticle energy as a function of the magnetic field,⁷¹

$$\mu = - \left(\frac{\partial E^\tau(k)}{\partial B} \right)_{B=0}, \quad (60)$$

to be understood as the left- or right-hand limit in the presence of a cusp. The magnetic moment may be measured through single-electron tunneling spectroscopy.⁵⁷

The dependence of quasiparticle band edges $E^\tau(k = 0)$ on φ is illustrated in Fig. 10 for both metallic (left panel) and semiconducting (right panel) tubes. The magnitudes of the slopes of quasiparticle bands (red [gray] lines) are enhanced with respect to noninteracting bands (black lines). While EI band edges of both metallic and semiconducting tubes have comparable slopes at the origin, they exhibit differences at large values of φ as the band edges of semiconducting tubes deviate from linearity.

The case of metallic nanotubes ($\nu = 0$) allows for an analytical treatment as the excitonic gap Δ is the same in both valleys, $E(k) \equiv E^\tau(k)$. Recalling that the magnetic field B along the tube axis enters both equations (51) and (57) through the field-dependent transverse wave vector [Eq. (5)],

$$k_{\nu=0}(0) = \frac{BLe}{2\hbar}, \quad (61)$$

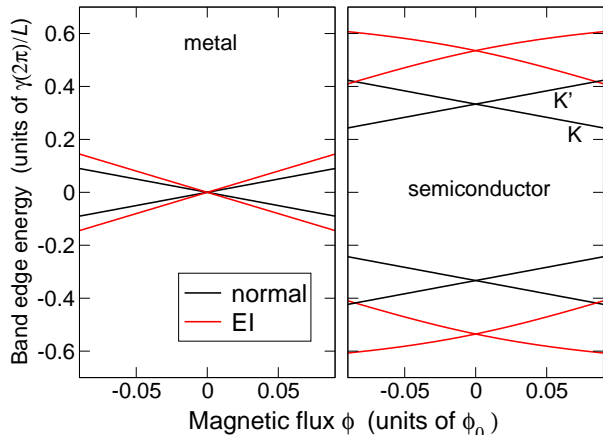


FIG. 10. (color online) Dependence of EI quasiparticle (non-interacting) band edges $E^\tau(k=0)$ [$\varepsilon^\tau(k=0)$] on the magnetic flux φ . Left panel: metal ($\nu=0$). Right panel: semiconductor ($\nu=1$). Here $\varphi = \phi/\phi_0$ is the ratio of the magnetic flux ϕ through the tube cross section to the magnetic flux quantum $\phi_0 = ch/e$, $a(2\pi/L) = 1$, and $w_2 = 150\gamma(2\pi/L)$. For the sake of comparison the weak-coupling results are used in both panels.

after derivation we obtain

$$\mu = \pm\mu_0 \left[\frac{\sinh\left(\frac{\pi}{2}\right)}{\sinh\left(\frac{2\pi\gamma}{W_0 + \Omega_0 w_2/(2L)}\right)} \right]. \quad (62)$$

Here the sign plus (minus) corresponds to the (anti)parallel orientation of the magnetic moment of the quasiparticle with respect to the magnetic field, and $\mu_0 = ev_F R/2c$ is the semiclassical value of the magnetic moment of the electron rotating around the tube circumference with Fermi velocity $v_F = \gamma/\hbar$ (Ref. 57).

In the noninteracting phase the term enclosed by square brackets in (62) is the unity, hence one recovers the semiclassical result $\mu = \pm\mu_0$. In the EI phase this value is increased by the factor in parentheses, in a fashion proportional to the excitonic gap Δ —at least for strong interaction. The dependence of μ on intervalley exchange interaction strength $(\Omega_0 w_2/2L)/\gamma$ in the EI phase is illustrated in Fig. 11, which highlights the excitonic enhancement with respect to μ_0 . The peculiar scaling of μ with R is the experimental hallmark of exciton condensation, as further discussed in Sec. XII (cf. Fig. 13). Note that the weak-coupling estimate of μ (dashed line in Fig. 11) tends to the horizontal asymptote $\mu = \pm\sqrt{3}\mu_0$ whereas the strong-coupling prediction (solid line) increases indefinitely with intervalley exchange interaction.

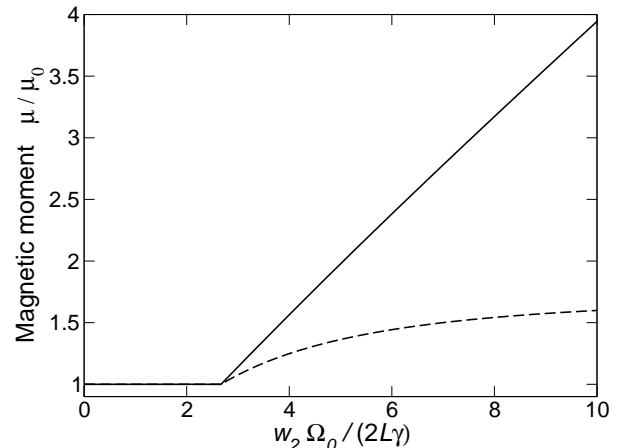


FIG. 11. Quasiparticle magnetic moment $|\mu|/\mu_0$ of a nominally metallic tube vs exchange interaction strength $(\Omega_0 w_2/2L)/\gamma$ at zero temperature. The dashed curve is the weak-coupling prediction. Here $W_0 = 1.33\gamma$ and μ_0 is the semiclassical estimate of the magnetic moment.

XI. WEAK PARAMAGNETISM OF THE EXCITON CONDENSATE

To shed light onto the unusual value of the magnetic moment of quasiparticles we consider the magnetization of the EI ground state, focusing on nominally metallic tubes ($\nu=0$) for the sake of clarity. We compute only the orbital magnetization M along the nanotube axis since the spin contribution is negligible, the Zeeman spin term coupling with the field being much smaller than the orbital coupling term.⁵⁷

The total magnetization M is the sum of the magnetic moments of filled one-electron levels, each moment being weighted by the level occupancy. All levels share approximately the same absolute value of the magnetic moment, μ_0 , whose sign is opposite for conduction and valence bands, respectively. This may be understood in a semiclassical picture,⁵⁷ as the transverse wave vector $k_{\nu=0}(0) \propto B$ along the circumferential direction x is the same for conduction and valence states whereas the corresponding group velocities $1/\hbar(\partial\varepsilon_\alpha/\partial k)_x$ have alternate signs. Therefore, all electrons in the conduction band rotate—say—anticlockwise around the tube circumference whereas those in the valence band rotate clockwise, as shown pictorially in Fig. 1(a). At finite wave vector k the magnetic moment $\mu_0(k)$ slightly departs from μ_0 due to the change in the group velocity:

$$\mu_0(k) = \frac{\mu_0}{\sqrt{1 + k^2/k_{\nu=0}^2(0)}}. \quad (63)$$

In terms of intraband Green functions, the magnetiza-

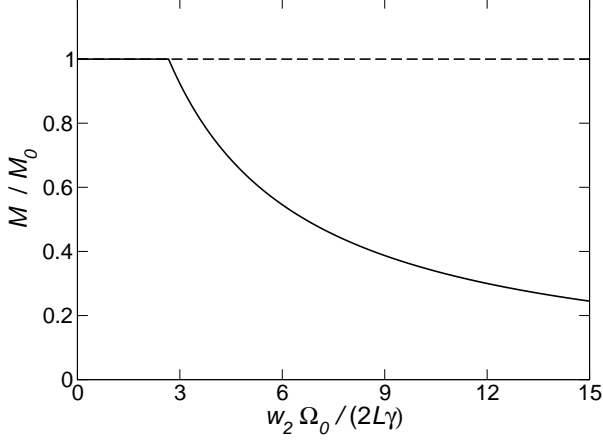


FIG. 12. Magnetization M of the excitonic insulator vs intervalley exchange interaction $(\Omega_0 w_2 / 2L) / \gamma$ (solid line). The dashed line is the magnetization M_0 of the noninteracting phase, which is metallic. Here $T = 0$ and $W_0 = 1.33\gamma$.

tion is

$$M = -i\hbar \sum_{\tau k} \mu_0(k) \sum_{\sigma} \left[G_{\sigma\sigma}^v(\tau k, t = 0-) - G_{\sigma\sigma}^c(\tau k, t = 0-) \right]. \quad (64)$$

Integrating over the frequency, we obtain

$$M = 4 \sum_k \mu_0(k) (u_k^2 - v_k^2), \quad (65)$$

where the coherence factors u_k and v_k are defined in analogy with the BCS theory of superconductivity:

$$u_k^2 = \frac{1}{2} \left(1 + \frac{\sqrt{\gamma^2 k^2 + \gamma^2 k_{\nu=0}^2(0)}}{\sqrt{\gamma^2 k^2 + \gamma^2 k_{\nu=0}^2(0) + |\Delta|^2}} \right), \quad (66)$$

$$v_k^2 = 1 - u_k^2.$$

The quantities u_k^2 and v_k^2 are the populations of valence- and conduction-band levels, respectively. In the noninteracting ground state the excitonic gap Δ vanishes, hence $u_k^2 = 1$, $v_k^2 = 0$, that is the valence band is filled and the conduction band empty, so one obtains $M_0 = \mu_0 ALB(e/\hbar c)$ (the subscript 0 identifies the noninteracting phase). Therefore, the tube is a paramagnet having susceptibility per unit length $\mu_0 L(e/\hbar c)$ and magnetization proportional to the semiclassical dipole μ_0 times the number of magnetic flux quanta piercing the tube surface AL . This scenario is illustrated in Fig. 1(a), with all electrons carrying their magnetic dipole aligned with the field B .

The condensation of excitons ($\Delta \neq 0$) decreases the magnitude of M with respect to M_0 , making the excitonic insulator a weak paramagnet as opposed to the normal

phase, according to

$$M = M_0 \frac{4\gamma}{W_0 + \Omega_0 w_2 / (2L)}, \quad (67)$$

which is valid for $W_0 + \Omega_0 w_2 / (2L) > 4\gamma$. The reason is that, as electron-hole pairs spontaneously form, electron states in the conduction band acquire a fractional occupation ($v_k^2 > 0$) as well as hole states in the valence band ($u_k^2 < 1$), as shown in Fig. 1(b), thus $M < M_0$. The magnetizations of noninteracting (dashed line) and EI (solid curve) phases are compared in Fig. 12 as a function of intervalley exchange interaction. The lower bound of the magnetization is $M = 0$, corresponding to the maximum exciton density allowed, the valence band being half-empty and the conduction band half-filled.

The quenching of magnetization causes an increase of the kinetic energy of the EI ground state that is compensated by the energy gain due to the condensation of excitons. In fact, it is easy to show that the kinetic energy increases linearly with the field whereas the interaction energy decreases quadratically to the leading order. This may be also seen by computing the work U done by the external field B to magnetize the tube, $U = \int B dM$. The difference ΔU between the magnetization work in the noninteracting and EI phases is the condensation energy of the excitonic insulator,

$$\Delta U = \mu_0 B^2 \frac{ALe}{2ch} \left[1 - \frac{4\gamma}{W_0 + \Omega_0 w_2 / (2L)} \right], \quad (68)$$

whose expression is valid for $W_0 + \Omega_0 w_2 / (2L) > 4\gamma$.

A finite amount of this condensation energy is released when creating a quasiparticle, i.e., an electron (hole) occupying a definite level k with unit probability. This is achieved by breaking the electron-hole pair of the condensate having amplitude u_k for the conduction level k being empty and v_k being occupied.

The quasiparticle energy $E(k)$ is defined as the change in the ground-state energy $E_0(N)$ of the system with N electrons when adding / removing one particle,⁶⁸ $E(k) = E_0(N \pm 1) - E_0(N)$. Therefore, $E(k)$ takes into account the released condensation energy per broken pair in terms of the excitonic gap Δ [Eq. (51)]. Similarly, the magnetic dipole per particle $\mu = -\partial E(k) / \partial B$ accounts for the increase of the ground-state magnetization when annihilating an exciton of the condensate. This explains the enhancement of μ with respect to the noninteracting value μ_0 [Eq. (62)].

The same rationale for the enhancement of the magnetic moment per quasiparticle is valid for semiconducting tubes ($\nu = \pm 1$), as the above argument may be applied separately to each valley in reciprocal space. The difference with respect to metallic tubes is that the EI ground state magnetization is now zero, since the bands in the two valleys exhibit opposite chiralities.

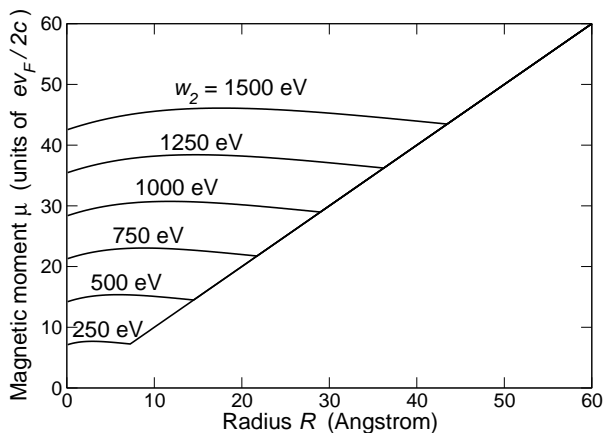


FIG. 13. Quasiparticle magnetic moment μ of a nominally metallic tube vs tube radius R , for different values of the intervalley contact interaction w_2 . Here $T = 0$ and $W_0 = 1.33\gamma$.

XII. RELATION TO EXPERIMENTS

The excitonic insulator phase of carbon nanotubes has two experimental signatures of genuine many-body origin that may be accessed by current experiments.

The first fingerprint is the enhancement of the electron magnetic moment μ measured by tunneling spectroscopy⁵⁷ with respect to the semiclassical value μ_0 , which was illustrated in Sec. X. According to formula (62), μ displays a peculiar dependence on the tube radius R , in contrast to the simple linear dependence of μ_0 . As shown in Fig. 13 for nominally metallic tubes, μ is almost independent from R for small values of the radius, exhibiting a plateau whose extension increases with the intervalley contact interaction w_2 . As the radius reaches the critical value of the transition from the EI to the normal phase, μ regains the familiar linear dependence from R . An important practical consequence of this prediction is that the radius of a small-diameter tube may not be inferred from a measure of μ , since only for R larger than the critical size the semiclassical formula $\mu_0 = e v_F R / 2c$ holds.

The second fingerprint is the increase of the quasiparticle gap of the EI phase with respect to the gap E_g of the noninteracting ground state. This occurs through the excitonic term Δ that adds quadratically to E_g , hence the EI gap may be written as

$$2\sqrt{(E_g/2)^2 + |\Delta|^2}. \quad (69)$$

Throughout this paper we have identified E_g as the gap due solely to tube chirality and/or axial magnetic field, $E_g/2 \equiv \gamma |k_\nu(0)|$. Nevertheless, the result (69) is generic to any energy gap that originates from the effective displacement of Dirac cone apexes with respect to allowed wave vectors in the Brillouin zone, including the small mass terms due to tube curvature, strain, and twists.^{35,36}

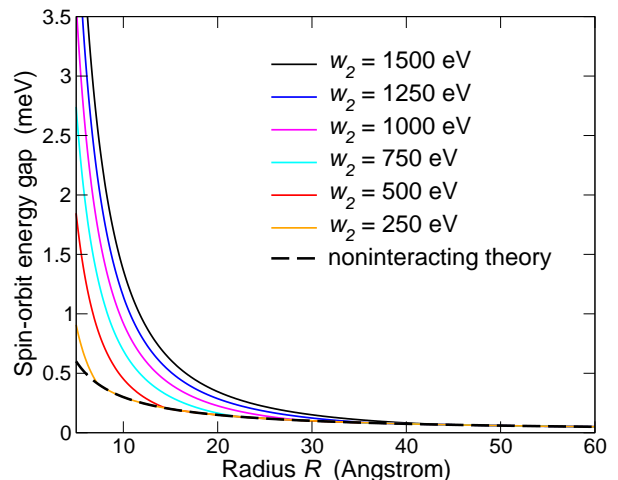


FIG. 14. (Color online) Transport gap induced by spin-orbit interaction in a nominally metallic tube vs tube radius R . The dashed line is the prediction of noninteracting theory, $E_g^{\text{SO}} = 3/(R [\text{\AA}])$ meV, whereas the solid lines are the gaps in the excitonic insulator phase for different values of the intervalley contact interaction w_2 . Here $T = 0$, $B = 0$, and $W_0 = 1.33\gamma$.

This holds also for the mass term induced by spin-orbit interaction in nominally metallic tubes.^{12,37,38} The spin-orbit correction to the noninteracting single-particles energies (8) and (11) takes the form

$$\varepsilon_\alpha^{\tau\sigma}(k) = s_\alpha \gamma \sqrt{k_{\nu=0}^2(n) + k^2}, \quad (70)$$

with the transverse momentum $k_{\nu=0}(n)$ being displaced by the spin-orbit term Δ_{SO} , with phase given by $\tau\sigma$,

$$k_{\nu=0}(n) = \frac{1}{R} (n + \varphi) + \frac{\Delta_{\text{SO}}}{\gamma R} \tau\sigma. \quad (71)$$

Here we ignore the rigid energy shift due to the recently discussed Zeeman-like term.^{12,72-74} Then, at zero field spin-orbit interaction opens a small spin-independent gap E_g^{SO} between conduction and valence bands, whose size is $E_g^{\text{SO}} = 2\Delta_{\text{SO}}/R$.

Figure 14 shows the spin-orbit gap enhanced by the excitonic order (solid lines) vs R . This is compared with the noninteracting spin-orbit gap E_g^{SO} , shown as a dashed curve (with⁸ $\Delta_{\text{SO}} = 1.5 \text{ meV}\cdot\text{\AA}$). Whereas at large R the gap is inversely proportional to the radius, consistently with the noninteracting theory, as R falls below the critical size the gap acquires a much stronger dependence on R , scaling like $1/R^2$.

Overall, the behavior of the spin-orbit gap exhibited in Fig. 14 complements that of the magnetic moment illustrated in Fig. 13, with both observables μ and E_g^{SO} being enhanced by an excitonic factor that scales as $1/R$. To derive the exact relation between μ and spin-orbit energy splittings requires to consider the case in which both

Reference	μ measured (meV/T)	R inferred (nm)	R measured (nm)	E_g^{SO} measured (μeV)	E_g^{SO} expected (μeV)	w_2 estimated (eV)	R predicted here (nm)
Kuemmeth 2008 ⁸	1.55	3.50	n.a.	370	110	1208	1.73
Jespersen 2011 ¹¹	0.63	1.45	n.a.	150	168	n.a.	1.45
Jespersen PRL 2011 ⁵⁹	0.87	2.65	n.a.	200	146	914.4	2.02
Churchill 2009 ⁹	0.33	0.75	n.a.	170	520	n.a.	0.75
Jhang 2010 ¹⁰	n.a.	n.a.	0.75	2500	520	1250	0.67
Steele 2012 ¹² device 1	1.60	3.60	1.50	3400	260	1242	0.57
Steele 2012 ¹² device 2	1.50	3.40	n.a.	1500	116	1173	0.84
Steele 2012 ¹² device 3	0.90	2.05	n.a.	1700	190	707.4	0.62

TABLE II. Comparison between predictions for the CNT excitonic insulator and available experimental data. The meaning of different entries is as follows: μ is the orbital magnetic moment measured through single-electron tunneling spectroscopy. The inferred radius R is obtained from the measured value of μ through the semiclassical formula $\mu_0 = ev_F R/2c$. The measured values of R are obtained from AFM experiments. The spin-orbit energy splitting E_g^{SO} is measured through single-electron tunneling spectroscopy in the conduction band. The expected value of E_g^{SO} is obtained from the inferred value of R (or from the measured value when available) according to the noninteracting theory of Ref. 12 (cf. Table S1). The intervalley contact interaction w_2 and the predicted value of R in the EI phase are evaluated through the procedure explained in the main text.

spin-orbit interaction and magnetic field are present, lifting spin and valley degeneracies of quasiparticle levels. This analysis will be presented elsewhere.

A. Comparison with available literature

Table II lists the magnetic moments and spin-orbit energy splittings reported for single-wall CNTs close to charge neutrality at low temperature (after Table S1 of Ref. 12). The second and third columns report respectively tunneling-spectroscopy data⁵⁷ for μ and corresponding values of R inferred through the semiclassical formula $\mu_0 = ev_F R/2c$. In all cases but two (Refs. 11 and 9) the inferred values exceed the actual values of R by a factor two or more, as realistic numbers fall in a range between 0.2 and 1.5 nm. This discrepancy is confirmed by available AFM measurements (fourth column), as it is the case of device 1 of Ref. 12, whose inferred radius of 3.6 nm is more than twice larger than the measured radius of 1.5 nm.

These data are presently not understood.⁶ A possible explanation is that the Fermi velocity v_F appearing in the expression for μ_0 has to be renormalized.⁵⁹ However, a correction of a factor two can hardly be justified, as state-of-the-art quasiparticle calculations, able to rationalize optical spectra, provide values of v_F comparable to the tight-binding estimate.⁷⁵ Besides, the effective-mass corrections to v_F predicted by (63) become significant only far from band edges.^{11,59}

In the spirit of Sec. VII, here we use the values of μ reported in the second column of Table II to estimate the intervalley exchange interaction parameter w_2 . First, from the inspection of the apparent magnitudes of R , we assign all inferred values but those of Refs. 11 and 9 to the EI phase. As shown in Fig. 13, we expect that the actual values of R fall somewhere in the region in which

μ exhibits a plateau. Then, to extract w_2 , we equate the experimental value of μ with that predicted at the transition point between EI and noninteracting phase, being representative of the values of μ over the whole plateau. The outcome of this procedure is reported in the seventh column of Table II, providing estimates for w_2 that vary between 700 and 1200 eV. To extract the actual tube radius we need a second, independent set of measurements, which is provided by spin-orbit data.

Table II shows available data for spin-orbit energy splittings (fifth column), together with their maximum sizes expected by noninteracting theory (sixth column), according to Ref. 12. The comparison highlights that measured data may exceed theoretical estimates by one order of magnitude, which has not been explained yet.¹² The listed experimental values have diverse origins, i.e., they are typically energy splittings separating excited electron states of both metallic and semiconducting tubes, ascribed to both Zeeman-like and orbital-like spin-orbit terms. Therefore, these data cannot be straightforwardly compared with the predictions of Fig. 14. Nevertheless, we use them as rough estimates of spin-orbit gaps in nominally metallic tubes.

Since in Table II we have now linked the samples to their values of w_2 (for the sample of Ref. 10 we assume $w_2 = 1250$ eV), we may plot the spin-orbit gap of each device versus R , similarly to the curves in Fig. 14. By intersecting each curve with the horizontal line that identifies the measured entry of E_g^{SO} , we eventually extract the value of R in the EI phase, which is tabulated in the last column. This number, systematically lower than the apparent value of R of column two, ranges between 0.6 and 2 nm, reasonably comparing with realistic values. This estimate provides an important consistency check of the theory.

B. The Caltech experiment

The claim of the observation of the Mott-Hubbard gap in nominally metallic CNTs by the Caltech group in 2009 relies on the idea of using the magnetic field to remove the noninteracting energy contribution E_g to the transport gap.¹⁶ The term E_g is generically ascribed to a small shift of the transverse wave vector (71), which may be fully counteracted by a properly chosen Aharonov-Bohm phase φ of like magnitude and opposite sign. At such critical value of the field the measured transport gap was found not to vanish, even after subtracting the energy contribution due to Coulomb blockade. Therefore, this inherent gap was interpreted as a genuine many-body effect.¹⁶

Since the opening of a many-body gap at $E_g = 0$ is peculiar to the Mott-Hubbard scenario (cf. Table I), it would appear that evidence rules out exciton condensation. However, the presence of spin-orbit interaction, which was overlooked in the analysis of Ref. 16, makes the EI scenario possible. This may be seen qualitatively from the spin-valley dependence of the transverse wave vector (71): If the gap E_g^{SO} in valley τ closes in the spin channel σ for a suitable value of φ , then it remains finite in the other channel $-\sigma$, with $E_g^{\text{SO}} = 4|\Delta_{\text{SO}}|$. Therefore, the noninteracting gap experienced by triplet excitons never vanishes.

Also, the observation of subgap neutral collective excitations reported in Ref. 16 might be consistent with the EI scenario (cf. Table I). These excitations are expected as phonon-like collective modes of the EI, either of acoustic or optical type, as well as spin density waves. These modes correspond to space-time fluctuations of the phase and magnitude of Δ or oscillations of the spin-polarization vector \mathbf{n} , respectively.^{47,48,76} The theory of EI collective excitations as well as the quantitative analysis of the data of Ref. 16 are left to future work.

XIII. CONCLUSIONS

In this work we have proposed that the ground state of an undoped carbon nanotube of small diameter might be an excitonic insulator. The condensate is made of triplet excitons that are stabilized by intervalley exchange interaction, which induces antiferromagnetic spin density wave order. The ultimate validation of this theory relies on the observation of the excitonic enhancement of both energy gap and magnetic moment of quasiparticles, which might have already been measured.

ACKNOWLEDGMENTS

We thank Shahal Ilani, Elisa Molinari, Daniele Varsano, Deborah Prezzi, and Ehud Altman for stimulating discussions. This work is supported by EU-FP7

Marie Curie initial training network INDEX and MIUR-PRIN2012 Project MEMO.

Appendix A: Generic solution of the Bethe-Salpeter equation for the lowest triplet exciton

In this Appendix we solve the Bethe-Salpeter equation (36) for the lowest triplet exciton in a semiconducting carbon nanotube ($\nu = \pm 1$) in the presence of an external magnetic field along the tube axis. The method is a generalization of the procedure explained in Sec. IV, which we work out numerically.

The generic solution of (36) is a bound state with distinct envelope functions in the two valleys,

$$\begin{aligned}\psi_{\text{K}}(y) &= \sin \theta \sqrt{\kappa_{\text{K}}} \exp(-\kappa_{\text{K}} |y|), \\ \psi_{\text{K}'}(y) &= \cos \theta \sqrt{\kappa_{\text{K}'}} \exp(-\kappa_{\text{K}'} |y|),\end{aligned}\quad (\text{A1})$$

with $0 \leq \theta \leq \pi/2$, whose energy is

$$\varepsilon_u = 2\gamma \sqrt{k_{\nu}(0)^2 - \kappa_{\text{K}}^2} = 2\gamma \sqrt{k_{-\nu}(0)^2 - \kappa_{\text{K}'}^2}. \quad (\text{A2})$$

The exciton energy ε_u is smaller than the minimum between the two valley-dependent energy gaps $2\gamma |k_{\nu}(0)|$ and $2\gamma |k_{-\nu}(0)|$. If these are equal (either the tube is metallic or the field is zero) than $\theta = \pi/4$ and one recovers the solution (19).

The boundary condition at the origin (22) now turns into the system of equations

$$\begin{aligned}\left[\gamma \sqrt{k_{\nu}(0)^2 - \kappa_{\text{K}}^2} - \gamma |k_{\nu}(0)| + \frac{\kappa_{\text{K}} W_0}{4} \right] \sin \theta \sqrt{\kappa_{\text{K}}} \\ = -\frac{\kappa_{\text{K}} \Omega_0 w_2}{8L} \cos \theta \sqrt{\kappa_{\text{K}'}} ,\end{aligned}\quad (\text{A3a})$$

$$\begin{aligned}\left[\gamma \sqrt{k_{-\nu}(0)^2 - \kappa_{\text{K}'}^2} - \gamma |k_{-\nu}(0)| + \frac{\kappa_{\text{K}'} W_0}{4} \right] \cos \theta \sqrt{\kappa_{\text{K}}} \\ = -\frac{\kappa_{\text{K}'} \Omega_0 w_2}{8L} \sin \theta \sqrt{\kappa_{\text{K}}} .\end{aligned}\quad (\text{A3b})$$

As the onset of the excitonic instability occurs for $\varepsilon_u = 0$, it is easy to show that the critical value of intervalley exchange interaction is given again by Eq. (38), $W_0 + \Omega_0 w_2 / (2L) = 4\gamma$, which implies

$$\tan \theta = \sqrt{\left| \frac{k_{-\nu}(0)}{k_{\nu}(0)} \right|}. \quad (\text{A4})$$

Solving system (A3) for κ_{K} and $\kappa_{\text{K}'}$ other than zero leads to the secular equation

$$\begin{aligned}\left[\gamma \sqrt{k_{\nu}(0)^2 - \kappa_{\text{K}}^2} - \gamma |k_{\nu}(0)| + \frac{\kappa_{\text{K}} W_0}{4} \right] \\ \times \left[\gamma \sqrt{k_{-\nu}(0)^2 - \kappa_{\text{K}'}^2} - \gamma |k_{-\nu}(0)| + \frac{\kappa_{\text{K}'} W_0}{4} \right] \\ - \kappa_{\text{K}} \kappa_{\text{K}'} \left(\frac{\Omega_0 w_2}{8L} \right)^2 = 0.\end{aligned}\quad (\text{A5})$$

We obtain the root of (A5) numerically, with both κ_K and $\kappa_{K'}$ explicit in terms of the unknown ε_u . This gives the exciton energy at arbitrary values of energy gaps, as illustrated in Fig. 5.

Appendix B: Generic solution of the EI gap equation

In this Appendix we solve the gap equation (53) for a semiconducting carbon nanotube ($\nu = \pm 1$) in the presence of an external magnetic field applied along the tube axis.

Paralleling the strategy of Sec. IX, we assume that the excitonic gap in each valley is much smaller than the corresponding noninteracting gap. Therefore, we may

expand the square roots entering (53) and obtain

$$\begin{aligned} -\frac{|\Delta(K)|^2}{\gamma |k_\nu(0)|} \varphi^K(k) &= 2\gamma \sqrt{k_\nu^2(0) + k^2} \varphi^K(k) \\ -\frac{1}{A} \sum_q W_0 \varphi^K(k+q) - \frac{1}{A} \sum_q \frac{\Omega_0 w_2}{2L} \varphi^{K'}(k+q), \\ -\frac{|\Delta(K')|^2}{\gamma |k_{-\nu}(0)|} \varphi^{K'}(k) &= 2\gamma \sqrt{k_{-\nu}^2(0) + k^2} \varphi^{K'}(k) \\ -\frac{1}{A} \sum_q W_0 \varphi^{K'}(k+q) - \frac{1}{A} \sum_q \frac{\Omega_0 w_2}{2L} \varphi^K(k+q). \end{aligned} \quad (B1)$$

This is identical to the Bethe-Salpeter equation (36) for a triplet exciton of energy

$$\varepsilon_u = -\frac{|\Delta(K)|^2}{\gamma |k_\nu(0)|} = -\frac{|\Delta(K')|^2}{\gamma |k_{-\nu}(0)|}. \quad (B2)$$

We exploit this identity to obtain the excitonic gap using the numerical results derived by the method explained in Appendix A.

-
- * massimo.rontani@nano.cnr.it; www.nano.cnr.it
- ¹ R. Saito, G. Dresselhaus, and M. S. Dresselhaus, *Physical Properties of Carbon Nanotubes* (Imperial College Press, London, 1998)
 - ² T. Ando, J. Phys. Soc. Jpn. **74**, 777 (2005)
 - ³ S. Ilani and P. L. McEuen, Ann. Rev. of Cond. Mat. Phys. **1**, 1 (2010)
 - ⁴ V. V. Deshpande, M. Bockrath, L. I. Glazman, and A. Yacoby, Nature **464**, 209 (2010)
 - ⁵ F. Kuemmeth, H. O. H. Churchill, P. K. Herring, and C. M. Marcus, Mater. Today **13**, 18 (2010)
 - ⁶ E. A. Laird, F. Kuemmeth, G. Steele, K. Grove-Rasmussen, J. Nygård, K. Flensberg, and L. P. Kouwenhoven, "Quantum transport in carbon nanotubes," (2014), arXiv:1403.6113
 - ⁷ J. Cao, Q. Wang, and H. Dai, Nature Mat. **4**, 745 (2005)
 - ⁸ F. Kuemmeth, S. Ilani, D. C. Ralph, and P. L. McEuen, Nature **452**, 448 (2008)
 - ⁹ H. O. H. Churchill, F. Kuemmeth, J. W. Harlow, A. J. Bestwick, E. I. Rashba, K. Flensberg, C. H. Stwertka, T. Taychatanapat, S. K. Watson, and C. M. Marcus, Phys. Rev. Lett. **102**, 166802 (2009)
 - ¹⁰ S. H. Jhang, M. Marganska, Y. Skourski, D. Preusche, B. Witkamp, M. Grifoni, H. van der Zant, J. Wosnitza, and C. Strunk, Phys. Rev. B **82**, 041404(R) (2010)
 - ¹¹ T. S. Jespersen, K. Grove-Rasmussen, J. Paaske, K. Muraki, T. Fujisawa, J. Nygård, and K. Flensberg, Nature Phys. **7**, 348 (2011)
 - ¹² G. A. Steele, F. Pei, E. A. Laird, J. M. Jol, H. B. Meerwaldt, and L. P. Kouwenhoven, Nature Commun. **4**, 1573 (2013)
 - ¹³ J. P. Cleuziou, N. V. N'Guyen, S. Florens, and W. Wernsdorfer, Phys. Rev. Lett. **111**, 136803 (2013)
 - ¹⁴ V. V. Deshpande and M. Bockrath, Nature Phys. **4**, 314 (2008)
 - ¹⁵ S. Pecker, F. Kuemmeth, A. Secchi, M. Rontani, D. C. Ralph, P. L. McEuen, and S. Ilani, Nature Phys. **9**, 576 (2013)
 - ¹⁶ V. V. Deshpande, B. Chandra, R. Caldwell, D. S. Novikov, J. Hone, and M. Bockrath, Science **323**, 106 (2009)
 - ¹⁷ J. Maultzsch, R. Pomraenke, S. Reich, E. Chang, D. Prezzi, A. Ruini, E. Molinari, M. S. Strano, C. Thomsen, and C. Lienau, Phys. Rev. B **72**, 241402(R) (2005)
 - ¹⁸ F. Wang, G. Dukovic, L. E. Brus, and T. Heinz, Science **308**, 838 (2005)
 - ¹⁹ S. Zaric, G. N. Ostojic, J. Shaver, J. Kono, O. Portugall, P. H. Frings, G. L. J. A. Rikken, M. Furis, S. A. Crooker, X. Wei, V. C. Moore, R. H. Hauge, and R. E. Smalley, Phys. Rev. Lett. **96**, 016406 (2006)
 - ²⁰ I. B. Mortimer and R. J. Nicholas, Phys. Rev. Lett. **98**, 027404 (2007)
 - ²¹ J. Shaver, J. Kono, O. Portugall, V. Krstić, G. L. J. A. Rikken, Y. Miyauchi, S. Maruyama, and V. Perebeinos, Nano Lett. **7**, 1851 (2007)
 - ²² A. Srivastava, H. Htoon, V. I. Klimov, and J. Kono, Phys. Rev. Lett. **101**, 087402 (2008)
 - ²³ R. Matsunaga, K. Matsuda, and Y. Kanemitsu, Phys. Rev. Lett. **101**, 147404 (2008)
 - ²⁴ O. N. Torrens, M. Zheng, and J. M. Kikkawa, Phys. Rev. Lett. **101**, 157401 (2008)
 - ²⁵ F. Wang, D. J. Cho, B. Kessler, J. Deslippe, P. J. Schuck, S. G. Louie, A. Zettl, T. F. Heinz, and Y. R. Shen, Phys. Rev. Lett. **99**, 227401 (2007)
 - ²⁶ C. L. Kane, L. Balents, and M. Fisher, Phys. Rev. Lett. **79**, 5086 (1997)
 - ²⁷ T. Giamarchi, *Quantum Systems in One Dimension* (Clarendon Press, Oxford (UK), 2004)
 - ²⁸ M. Bockrath, D. H. Cobden, J. Lu, A. G. Rinzler, R. E. Smalley, L. Balents, and P. L. McEuen, Nature **397**, 598 (1999)
 - ²⁹ H. Ishii, H. Kataura, H. Shiozawa, H. Yoshioka, H. Otsubo, Y. Takayama, T. Miyahara, S. Suzuki, Y. Achiba,

- M. Nakatake, T. Narimura, M. Higashiguchi, K. Shimanda, H. Namatame, and M. Taniguchi, *Nature* **426**, 540 (2003)
- ³⁰ L. Balents and M. P. A. Fisher, *Phys. Rev. B* **55**, 11973(R) (1997)
- ³¹ R. Egger and A. O. Gogolin, *Phys. Rev. Lett.* **79**, 5082 (1997)
- ³² L. S. Levitov and A. M. Tsvelik, *Phys. Rev. Lett.* **90**, 016401 (2003)
- ³³ R. M. Konik, *Phys. Rev. Lett.* **106**, 136805 (2011)
- ³⁴ A. Secchi and M. Rontani, *Phys. Rev. B* **85**, 121410(R) (2012)
- ³⁵ C. L. Kane and E. J. Mele, *Phys. Rev. Lett.* **78**, 1932 (1997)
- ³⁶ J. Charlier, X. Blase, and S. Roche, *Rev. Mod. Phys.* **79**, 677 (2007)
- ³⁷ T. Ando, *J. Phys. Soc. Jpn.* **69**, 1757 (2000)
- ³⁸ D. Huertas-Hernando, F. Guinea, and A. Brataas, *Phys. Rev. B* **74**, 155426 (2006)
- ³⁹ N. F. Mott and R. Peierls, *Proc. Phys. Soc.* **49**, 72 (1937)
- ⁴⁰ N. F. Mott, *Phil. Mag.* **6**, 287 (1961)
- ⁴¹ N. F. Mott, *Rev. Mod. Phys.* **40**, 677 (1968)
- ⁴² A. Auerbach, *Interacting Electrons and Quantum Magnetism* (Springer-Verlag, New York, 1994)
- ⁴³ Y. A. Krotov, D. Lee, and S. G. Louie, *Phys. Rev. Lett.* **78**, 4245 (1997)
- ⁴⁴ A. A. Nersesyan and A. M. Tsvelik, *Phys. Rev. B* **68**, 235419 (2003)
- ⁴⁵ L. V. Keldysh and Y. V. Kopae, *Fiz. Tverd. Tela.* **6**, 2791 (1964), [*Sov. Phys. Solid State* **6**, 2219 (1965)]
- ⁴⁶ A. N. Kozlov and L. A. Maksimov, *Zh. Eksp. i Teor. Fiz.* **48**, 1184 (1965), [*Sov. Phys.-JETP* **21**, 790 (1965)]
- ⁴⁷ D. Jérôme, T. M. Rice, and W. Kohn, *Phys. Rev.* **158**, 462 (1967)
- ⁴⁸ B. I. Halperin and T. M. Rice, *Solid State Phys.* **21**, 115 (1968)
- ⁴⁹ W. Kohn, in *Many-body physics*, edited by C. de Witt and R. Balian (Gordon and Breach, New York, 1968) p. 351
- ⁵⁰ B. A. Volkov, Y. V. Kopae, and A. I. Rusinov, *Zh. Eksp. i Teor. Fiz.* **68**, 1899 (1975), [*Sov. Phys.-JETP* **41**, 952 (1976)]
- ⁵¹ M. Rontani and L. J. Sham, in *Novel Superfluids Volume 2*, International Series of Monographs on Physics, Vol. 157, edited by K. H. Bennemann and J. B. Ketterson (Oxford University Press, Oxford, UK, 2014) Chap. 19, pp. 423–474, preprint at arXiv:1301.1726
- ⁵² T. Ando, *J. Phys. Soc. Jpn.* **66**, 1066 (1997)
- ⁵³ R. R. Hartmann, I. A. Shelykh, and M. E. Portnoi, *Phys. Rev. B* **84**, 035437 (2011)
- ⁵⁴ T. Ando, *J. Phys. Soc. Jpn.* **75**, 024707 (2006)
- ⁵⁵ H. Zhao and S. Mazumdar, *Phys. Rev. Lett.* **93**, 157402 (2004)
- ⁵⁶ C. D. Spataru, S. Ismail-Beigi, L. X. Benedict, and S. G. Louie, *Phys. Rev. Lett.* **92**, 077402 (2004)
- ⁵⁷ E. D. Minot, Y. Yaish, V. Sazonova, and P. L. McEuen, *Nature* **428**, 536 (2004)
- ⁵⁸ P. D. Jarillo-Herrero, J. Kong, H. S. J. van der Zant, C. Dekker, L. P. Kouwenhoven, and S. de Franceschi, *Phys. Rev. Lett.* **94**, 156802 (2005)
- ⁵⁹ T. S. Jespersen, K. Grove-Rasmussen, K. Flensberg, J. Paaske, K. Muraki, T. Fujisawa, and J. Nygård, *Phys. Rev. Lett.* **107**, 186802 (2011)
- ⁶⁰ H. Ajiki and T. Ando, *J. Phys. Soc. Jpn.* **62**, 1255 (1993)
- ⁶¹ A. Secchi and M. Rontani, *Phys. Rev. B* **88**, 125403 (2013)
- ⁶² W. Greiner, B. Müller, and J. Rafelski, *Quantum Electrodynamics of Strong Fields* (Springer Verlag, Berlin, 1985)
- ⁶³ V. M. Pereira, J. Nilsson, and A. H. Castro Neto, *Phys. Rev. Lett.* **99**, 166802 (2007)
- ⁶⁴ A. V. Shytov, M. I. Katsnelson, and L. S. Levitov, *Phys. Rev. Lett.* **99**, 236801 (2007)
- ⁶⁵ A. V. Shytov, M. I. Katsnelson, and L. S. Levitov, *Phys. Rev. Lett.* **99**, 246802 (2007)
- ⁶⁶ Y. Wang, D. Wong, A. V. Shytov, V. W. Brar, S. Choi, Q. Wu, H. Tsai, W. Regan, A. Zettl, R. K. Kawakami, S. G. Louie, L. S. Levitov, and M. F. Crommie, *Science* **340**, 734 (2013)
- ⁶⁷ P. A. Maksym and H. Aoki, *Phys. Rev. B* **88**, 081406(R) (2013)
- ⁶⁸ A. A. Abrikosov, L. P. Gorkov, and I. E. Dzyaloshinski, *Methods of quantum field theory in statistical physics* (Dover, New York, 1975)
- ⁶⁹ J. Bardeen, L. N. Cooper, and J. R. Schrieffer, *Phys. Rev.* **108**, 1175 (1957)
- ⁷⁰ P. G. de Gennes, *Superconductivity of metals and alloys* (Westview Press, Boulder (Colorado), 1999)
- ⁷¹ N. W. Ashcroft and N. D. Mermin, *Solid State Physics* (Saunders College Publishing, Fort Worth, 1976)
- ⁷² W. Izumida, K. Sato, and R. Saito, *J. Phys. Soc. Jpn.* **78**, 074707 (2009)
- ⁷³ J. Jeong and H. Lee, *Phys. Rev. B* **80**, 075409 (2009)
- ⁷⁴ J. Klinovaja, M. Schmidt, B. Braunecker, and D. Loss, *Phys. Rev. B* **84**, 085452 (2011)
- ⁷⁵ S. Choi, J. Deslippe, R. B. Capaz, and S. G. Louie, *Nano Lett.* **13**, 54 (2013)
- ⁷⁶ E. Bascones, A. A. Burkov, and A. H. MacDonald, *Phys. Rev. Lett.* **89**, 086401 (2002)